Towards physiologically meaningful water-use efficiency estimates from eddy covariance data

Accepted version

(with Permission and Acknowledgement,
Global Change Biology Oct. 11., 2017)

Jürgen Knauer, Sönke Zaehle, Belinda E. Medlyn, Markus Reichstein, Christopher A. Williams, Mirco Migliavacca, Martin G. De Kauwe, Christiane Werner, Claudia Keitel, Pasi Kolari, Jean-Marc Limousin, Maj-Lena Linderson

Published in: Global Change Biology

Towards physiologically meaningful water-use efficiency estimates from eddy covariance data

Jürgen Knauer[1,2,3] | Sönke Zaehle[1,4] | Belinda E. Medlyn[3] | Markus Reichstein[1,4] |
Christopher A. Williams[5] | Mirco Migliavacca[1] | Martin G. De Kauwe[6,7] |
Christiane Werner[8] | Claudia Keitel[9] | Pasi Kolari[10] | Jean-Marc Limousin[11] |
Maj-Lena Linderson[12]

[1]Department of Biogeochemical Integration, Max Planck Institute for Biogeochemistry, Jena, Germany

[2]International Max Planck Research School for Global Biogeochemical Cycles (IMPRS-gBGC), Jena, Germany

[3]Hawkesbury Institute for the Environment, Western Sydney University, Richmond, NSW, Australia

[4]Michael-Stifel-Center Jena for Data-Driven and Simulation Science, Jena, Germany

[5]Graduate School of Geography, Clark University, Worcester, MA, USA

[6]Department of Biological Science, Macquarie University, North Ryde, NSW, Australia

[7]ARC Centre of Excellence for Climate Extremes, University of New South Wales, Sydney, NSW, Australia

[8]Department of Ecosystem Physiology, University of Freiburg, Freiburg, Germany

[9]School of Life and Environmental Science, University of Sydney, Brownlow Hill, NSW, Australia

[10]Department of Physics, University of Helsinki, Helsinki, Finland

[11]Centre d'Ecologie Fonctionnelle et Evolutive, Université de Montpellier, Montpellier, France

[12]Department of Physical Geography and Ecosystem Science, Lund University, Lund, Sweden

Correspondence
Jürgen Knauer, Department of Biogeochemical Integration, Max Planck Institute for Biogeochemistry, Jena, Germany.
Email: jknauer@bgc-jena.mpg.de

Abstract

Intrinsic water-use efficiency (iWUE) characterizes the physiological control on the simultaneous exchange of water and carbon dioxide in terrestrial ecosystems. Knowledge of iWUE is commonly gained from leaf-level gas exchange measurements, which are inevitably restricted in their spatial and temporal coverage. Flux measurements based on the eddy covariance (EC) technique can overcome these limitations, as they provide continuous and long-term records of carbon and water fluxes at the ecosystem scale. However, vegetation gas exchange parameters derived from EC data are subject to scale-dependent and method-specific uncertainties that compromise their ecophysiological interpretation as well as their comparability among ecosystems and across spatial scales. Here, we use estimates of canopy conductance and gross primary productivity (GPP) derived from EC data to calculate a measure of iWUE (G_1, "stomatal slope") at the ecosystem level at six sites comprising tropical, Mediterranean, temperate, and boreal forests. We assess the following six mechanisms potentially causing discrepancies between leaf and ecosystem-level estimates of G_1: (i) non-transpirational water fluxes; (ii) aerodynamic conductance; (iii) meteorological deviations between measurement height and canopy surface; (iv) energy balance non-closure; (v) uncertainties in net ecosystem exchange partitioning; and (vi) physiological within-canopy gradients. Our results demonstrate that an unclosed energy balance caused the largest uncertainties, in particular if it was associated with erroneous latent heat flux estimates. The effect of aerodynamic conductance on G_1 was sufficiently captured with a simple representation. G_1 was found to be less sensitive to meteorological deviations between canopy surface and measurement height and, given that data are appropriately filtered, to non-transpirational water fluxes. Uncertainties in the derived GPP and physiological within-canopy gradients and their implications for parameter estimates at leaf and ecosystem level are discussed. Our results highlight the importance of adequately considering the sources of uncertainty outlined here when EC-derived water-use efficiency is interpreted in an ecophysiological context.

KEYWORDS

aerodynamic conductance, canopy gradients, eddy covariance, energy imbalance, intrinsic water-use efficiency, Penman–Monteith equation, slope parameter, surface conductance

1 | INTRODUCTION

Water-use efficiency (WUE) is an important vegetation property which characterizes the coupling of the water and carbon cycles at the leaf to global scales (Beer et al., 2009; Denmead, Dunin, Wong, & Greenwood, 1993; Farquhar, Hubick, Condon, & Richards, 1989; Ito & Inatomi, 2012). Understanding the physiological mechanisms that modulate WUE and being able to predict its future behavior in a changing environment is a fundamental challenge. Since the common formulation for WUE—the ratio of carbon gain to water loss—is affected by both physiological and environmental factors, alternative WUE metrics are useful that aim to extract the biological component of WUE. Such metrics have the advantage of being readily comparable across atmospheric conditions and across sites, and their dynamics can be more directly linked to the underlying physiological mechanisms. For example, many authors replace actual WUE (net photosynthesis (A_n)/transpiration) with the intrinsic WUE (iWUE = A_n/stomatal conductance (g_s)) (Osmond, Björkman, & Anderson, 1980; Schulze & Hall, 1982). However, iWUE is still indirectly dependent on environmental conditions, particularly vapor pressure deficit (VPD) and atmospheric CO_2 concentration (C_a). A metric that accounts for variations in these conditions is the "stomatal slope" or "slope coefficient" ("g_1" of the optimal stomatal model derived by Medlyn et al. (2011)). This parameter is inversely related to the marginal carbon cost of water to the plant and is calculated as the slope of the relationship between g_s and A_n, normalized for VPD and CO_2 concentration (Medlyn et al., 2011). g_1 is inversely related to intrinsic water-use efficiency (iWUE), and higher values of g_1 are associated with higher intercellular CO_2 concentrations (C_i). By accounting for confounding atmospheric factors, g_1 has been shown to provide valuable insights into the ecophysiological functioning of vegetation and its water-use strategy. It could, for instance, be related to wood density, which is a proxy for various plant hydraulic traits (Lin et al., 2015). g_1 is further, and in its original meaning, the key model parameter in stomatal conductance formulations embedded in ecosystem and Earth system models (Ball, Woodrow, & Berry, 1987; Leuning, 1995; Medlyn et al., 2011). Thus, knowledge on the variation of g_1 with climate and vegetation types is essential for understanding and modeling the physiological basis of present and future terrestrial water–carbon relations.

Values of g_1 are usually inferred from gas exchange measurements on individual leaves using transparent or lighted chambers. These instruments determine A_n and g_s from gas concentration changes within the chamber and provide simultaneous measurements of CO_2 concentration and humidity at the leaf surface, information from which g_1 can be readily inferred. One advantage of this measurement setup is that it provides conditions in which feedbacks with the physical environment (e.g., leaf boundary layer conductance) are largely controlled; thus, the information gained can be considered as purely physiological —though pitfalls exist (see Long & Bernacchi, 2003). One disadvantage of the method is that it is laborious and time-consuming, with the consequence that measurements are often restricted to a few days and to a small selection of leaves, usually located at the top of the canopy. As a consequence, leaf gas exchange measurements and resulting g_1 estimates are prone to spatial and temporal sampling biases.

Inferring g_1 from gas exchange measurements at the ecosystem scale with the eddy covariance (EC) technique (e.g., Aubinet et al., 1999) offers the potential to circumvent these biases. This method overcomes the main limitations of leaf-level data as it provides non-invasive, continuous, and long-term measurements of carbon, water, and energy fluxes that integrate an entire ecosystem. In principle, g_1 can be estimated from EC data in the same manner as at the leaf level if A_n and g_s are replaced by their ecosystem-level analogs and meteorological conditions at the leaf level with those measured at the flux tower (Medlyn et al., 2017). Ecosystem-integrated g_s, i.e., canopy conductance (G_c), is commonly derived as surface conductance (G_s) from the inverted Penman–Monteith (PM) equation, and ecosystem net photosynthesis can be approximated by gross primary productivity (GPP) as derived from measured net ecosystem exchange (NEE) of CO_2. G_1 (capital letters denote ecosystem-level quantities in this study) at ecosystem level constitutes a WUE-related ecosystem functional property according to Reichstein, Bahn, Mahecha, Kattge, and Baldocchi (2014) and has the advantage of representing a spatial and temporal integration of vegetation gas exchange, which supposedly yields more robust and representative WUE characteristics of an ecosystem than leaf gas exchange data. This aspect is especially relevant when the vegetation is of complex vertical structure or composed of multiple species with different physiological traits, in which case it is challenging to adequately represent the entire vegetation community with point measurements.

One challenge associated with EC data is that the measured fluxes are affected by physical feedback mechanisms that hinder conclusions about the underlying physiological mechanisms, an aspect that is generally of increasing importance when the scale of measurement is increased, e.g., from leaf to ecosystem (Anderson, Kustas, & Norman, 2003; Jarvis & McNaughton, 1986; Knauer et al., 2017). With the fluxes and meteorological variables measured a few meters above the canopy, an additional aerodynamic conductance (G_a) term has to be considered. Further, the EC system is unable to distinguish purely physical (i.e., evaporation) from physiologically controlled (i.e., transpiration) water fluxes. EC data are also subject to method-specific measurement errors and uncertainties. In particular, the measured energy fluxes often do not close the energy balance (Leuning, Van Gorsel, Massman, & Isaac, 2012; Wilson et al., 2002), and the partitioning of NEE into its component fluxes involves considerable uncertainties (Desai et al., 2008; Reichstein et al., 2005; Wehr et al., 2016). In addition, possible within-canopy gradients of g_1 cannot be directly resolved with EC measurements alone.

These aspects are especially relevant in the context of a recent study that found discrepancies between leaf- and EC-based estimates of g_1 and its patterns across vegetation types (Medlyn et al., 2017). These mismatches are unlikely to result from inadequate scaling procedures of WUE from leaf to ecosystem (Launiainen, Katul, Kolari, Vesala, & Hari, 2011; Linderson et al., 2012), but might in

large parts be caused by methodological uncertainties in the EC data and conceptual differences between the two data sources. Thus, identifying and quantifying the potential effects of these uncertainties will be a crucial first step to reconcile estimates across scales and enable a consistent use of the two data sources in modeling and observational studies.

Here, we analyze the sensitivity of G_1 to the factors outlined above at six forest ecosystems and compare it to leaf-level g_1 estimates at the same location. The objective of this study is to quantify the effects of confounding nonphysiological factors on ecosystem-level G_1, with the ultimate goal of deriving a physiologically meaningful WUE parameter from EC measurements that is analogous to leaf-level estimates. Such information can be used to (i) parameterize and evaluate large-scale models, (ii) obtain a characterization of ecosystem-level iWUE that is readily comparable across locations differing in their environmental conditions, and (iii) compare estimated vegetation gas exchange parameters across scales.

2 | MATERIALS AND METHODS

2.1 | Leaf-level estimates of g_1

Gas exchange measurements at leaf level are taken from previous studies (Table 1) and are in parts also included in the database compiled by Lin et al. (2015). Data are publicly available under https://bitbucket.org/gsglobal/leafgasexchange. Measurements were made with standard instruments mostly at the top third of the canopy for the dominant species at the site. For the analysis, the unified stomatal optimization model (Medlyn et al., 2011) was used:

$$g_s = g_0 + 1.6\left(1 + \frac{g_1}{\sqrt{D_s}}\right)\frac{A_n}{c_s} \qquad (1)$$

where g_0 is the minimum stomatal conductance (mol m^{-2} s^{-1}), g_1 is the stomatal slope parameter (kPa$^{0.5}$), and A_n is net photosynthesis (μmol m^{-2} s^{-1}). D_s is the vapor pressure deficit (kPa), and c_s is the CO_2 concentration (ppm), both at the leaf surface. g_1 was estimated from Equation (1) using nonlinear, iteratively reweighted least squares based on the R-package *robustbase* (Maechler et al., 2016). As in Lin et al. (2015), g_0 was set to 0 for the entire analysis, as (i) the physiological meaning of a statistically fitted g_0 is unclear (e.g., Barnard & Bauerle, 2013), and (ii) g_0 correlates with g_1, thus simultaneous estimation of both parameters would hamper the comparison of g_1 across datasets and sites.

2.2 | Ecosystem-level estimates of surface conductance and G_1

We analyzed EC data from six flux tower sites within the FLUXNET network, where colocated leaf-level measurements were available (Table 1). The EC data were taken from the FLUXNET2015 dataset (http://fluxnet.fluxdata.org/data/fluxnet2015-dataset/; accessed on 04.07.2016) and are at half-hourly or hourly resolution. The sites comprise one evergreen needle-leaf forest (FI-Hyy), two deciduous broadleaf forests (DK-Sor, US-Ha1), two evergreen broadleaf forests (AU-Tum, FR-Pue), and one evergreen tropical forest (GF-Guy). Flux data underwent standard processing, including friction velocity (u_*) filtering (Papale et al., 2006), gap filling, and flux partitioning (Reichstein et al., 2005). Only measured flux data were used.

TABLE 1 Characteristics of eddy covariance sites and colocated leaf-level measurements used in this study

Site	Climate[a]	Forest type	Max. LAI	Canopy height (m)	Reference EC site	Leaf-level g_1 (kPa$^{0.5}$)	Species sampled	Reference leaf-level data
AU-Tum	Cfb	Broadleaf evergreen	2.4	40	Leuning, Cleugh, Zegelin, and Hughes (2005)	3.7	*Eucalyptus delegatensis*	Medlyn, Pepper, O'Grady, and Keith (2007)
DK-Sor	Cfb	Broadleaf deciduous	4.5	25	Pilegaard, Ibrom, Courtney, Hummelshøj, and Jensen (2011)	4.0	*Fagus sylvatica*	Linderson et al. (2012)
FI-Hyy	Dfc	Needle-leaf evergreen	3.3	14	Vesala et al. (2005)	1.8	*Pinus sylvestris*	Kolari, Lappalainen, Hänninen, and Hari (2007)
FR-Pue	Csa	Broadleaf evergreen	3.3	5.5	Rambal et al. (2003)	1.6	*Quercus ilex*	Martin-StPaul et al. (2012)
GF-Guy	Af	Tropical evergreen	7.0[b]	35	Bonal et al. (2008)	4.4	77 species	J. Zaragoza-Castells, P. Meir, O. K. Atkin, Unpublished
US-Ha1	Dfb	Broadleaf deciduous	4.9	23	Urbanski et al. (2007)	4.9	*Acer rubrum*, *Betula alleghaniensis*, *Betula papyrifera*, *Quercus rubra*	Bassow and Bazzaz (1997)

[a]Köppen-Geiger climate classification (Af = equatorial, rainforest; Cfb = humid, warm temperate, warm summer; Csa = summer dry, warm temperate, hot summer; Dfb = cold, humid, warm summer; Dfc = cold, humid, cold summer).
[b]Plant area index.

Eddy covariance measurements were analyzed within a "big-leaf" model framework, in which vegetation is represented as a uniform, single plane, acting as the only flux source and sink in the ecosystem (e.g., Raupach & Finnigan, 1988). For the purpose of this study, a data-oriented, top-down approach based on the big-leaf framework was preferred over more detailed representations of the ecosystem, such as two-layer (vegetation–soil, e.g., Shuttleworth & Wallace, 1985) or dual-source models (sun–shade, e.g., de Pury & Farquhar, 1997) as these representations would require additional parameterization that cannot be obtained from single-level flux measurements.

Bulk surface conductance (G_s, m/s) was calculated from the inverted Penman–Monteith (PM) equation (Monteith, 1965):

$$G_s = \frac{\lambda E G_a \gamma}{s(R_n - G - S) + \rho c_p G_a D_a - \lambda E(s + \gamma)} \quad (2)$$

where λE is the latent heat flux (W/m^2), G_a is the bulk aerodynamic conductance for water vapor (m/s), γ is the psychrometric constant (Pa/K), s is the slope of the saturation vapor pressure curve (Pa/K), R_n is the net radiation (W/m^2), G is the ground heat flux (W/m^2), S is the sum of all energy storage fluxes (W/m^2), ρ is the air density (kg/m^3), c_p is the heat capacity of dry air (J kg^{-1} K^{-1}), and D_a is the air vapor pressure deficit (Pa). For some sites, G was measured with heat flux plates, whereas measurements of S were not available and set to 0 for all sites. The PM equation was applied at the half-hourly or hourly time-scale, thereby accounting for sub-diurnal variations in meteorological drivers. The approach is further based on similar assumptions as the EC technique (see, e.g., van Dijk et al., 2015 and references therein). G_s subsumes canopy conductance (G_c), as well as conductances from the soil and water intercepted by the canopy. Consequently, G_s is only a physiologically meaningful quantity ($G_s \approx G_c$) in time periods when vegetation is active, and the vegetation and soil surfaces are not wet. To ensure this to be the case, precipitation events, as well as the subsequent 48 hr, were excluded, and the analysis was restricted to daylight conditions (PPFD > 200 μmol m^{-2} s^{-1}) and to time periods within the growing season. Data were considered to be in the growing season when smoothed (15-day moving average) daily GPP exceeded half of the 95th percentile of all daily GPP values in a year (e.g., Fig. S1). Further filtering criteria included the following: air temperature >5°C, relative humidity <95%, $\lambda E > 0$ W/m^2, and $(R_n - G) > 0$ W/m^2. A site- and year-specific u_* threshold, as provided by the FLUXNET2015 dataset, was applied. Atmospheric CO_2 data were processed as described in Medlyn et al. (2017). Analysis steps performed in this study are available in the language R under https://bitbucket.org/juergenknauer/g1_leaf_ecosystem.

Ecosystem-level G_1 was calculated in the same manner as at the leaf level (Equation 1) but with g_s and A_n replaced by G_s and GPP (representing carboxylation minus photorespiration), respectively (Equation 3, data shown in Figs S2 and S3). Further, D_s and c_s were replaced by the respective measurements (D_a and C_a) at the flux tower:

$$G_s = G_0 + 1.6\left(1 + \frac{G_1}{\sqrt{D_a}}\right)\frac{\text{GPP}}{C_a} \quad (3)$$

G_1 in Equation (3) was determined on an annual basis using the same nonlinear regression method as for the determination of g_1 at leaf level.

2.3 | Factors affecting G_1 estimates

2.3.1 | Non-transpirational water fluxes

G_s as calculated from Equation (2) is affected by both transpiration and solely physically driven water fluxes (i.e., bare soil and interception evaporation); thus, G_c and G_1 are expected to be increasingly overestimated with increasing contribution of non-transpirational water fluxes to ET (Paw & Meyers, 1989). To analyze the sensitivity of G_1 to these contributions, we calculated G_1 for successively increasing time periods following a rainfall event. Time after rainfall is considered as an inverse proxy for the contribution of physical water fluxes to ET, which have been observed to decrease exponentially with time after rainfall (e.g., Kelliher et al., 1998), but not in all ecosystems (e.g., Dubbert et al., 2014). Since dew evaporation is, unlike soil and interception evaporation, not necessarily excluded by the rainfall filter, we additionally tested the effect of a simple dew evaporation filter on estimated annual values of G_1. The dew filter was applied if the likelihood of dew evaporation was high, which was considered the case if relative humidity exceeded 95% and the radiation balance turned negative ($R_n < 0$ W/m^2) at night. If these conditions were met, the PPFD threshold was raised to 600 μmol m^{-2} s^{-1} in the following morning.

2.3.2 | Aerodynamic conductance

The bulk aerodynamic conductance for water vapor (G_a) between the evaporating surface and the measurement height of the flux is an integral part of the PM equation (Equation 2). G_a can be conceptualized as the inverse of two resistances in series: $G_a = 1/R_a = (R_{aM} + R_b)^{-1}$, where R_{aM} is the turbulent aerodynamic resistance for momentum, and R_b is the (bulk) canopy boundary layer resistance or "excess resistance" (Verma, 1989).

We tested the effect of calculating G_a in Equation (2) using three different approaches of increasing complexity:

1. G_a set to infinity, corresponding to the assumption that the ecosystem is aerodynamically fully coupled to the atmosphere:

$$G_{a,\text{fcoupled}} = \infty \quad (4)$$

2. G_a calculated from wind speed u (m/s) and friction velocity u_* (m/s) under the assumption of a logarithmic wind profile above the canopy. R_b follows an empirical dependence on u_* according to Thom (1972):

$$1/G_{a,\text{empGb}} = \frac{u}{u_*^2} + 6.2u_*^{0.67} \quad (5)$$

Note that the first term of Equation (5) implicitly accounts for the effects of atmospheric stability on G_a.

3. As Equation (5) but with the empirical R_b model replaced by a physically based formulation according to Su, Schmugge, Kustas, and Massman (2001), a simplification of the model developed by Massman (1999):

$$1/G_{a,physGb} = \frac{u}{u_*^2} + \frac{\frac{kC_d}{4C_t\frac{u_z}{u(z_h)}}f_c^2 + kB_s^{-1}(1-f_c)^2}{ku_*} \tag{6}$$

where $k = 0.41$ is the von Kármán constant, C_d is a foliage drag coefficient, assumed constant with a value of 0.2 (Massman, 1999), C_t is the heat transfer coefficient of the leaf, f_c is fractional canopy cover, $u(z_h)$ is wind speed at canopy height (m/s), and B_s^{-1} is the inverse Stanton number for bare soil surface. C_t depends primarily on the leaf characteristic dimension D_l (m; values are taken from the literature, Table S1), and f_c was estimated from LAI (for further details, see Supporting Information).

To test the sensitivity of G_1 to different formulations of G_a, G_s (Equation 2) and G_1 (Equation 3) were calculated with G_a given by Equations (4)–(6). Throughout the following analysis, $G_{a,empGb}$ (Equation 5) was used.

2.3.3 | Meteorological deviations between measurement height and canopy surface

A finite G_a causes the meteorological conditions at the canopy surface to differ from those measured a certain distance above the canopy (e.g., Grantz & Meinzer, 1990). These deviations are important to consider since the conditions at the canopy surface are physiologically more relevant than those in the air above the canopy. Obtaining representative measurements of canopy surface micrometeorology is challenging, but surface temperature and humidity can be readily inferred from the inverted bulk transfer equations of sensible and latent heat if an estimate of G_a is available. Aerodynamic canopy surface temperature (T_0) is then given by:

$$T_0 = T_a + \frac{H}{\rho G_a c_p} \tag{7}$$

where T_a is air temperature (°C) measured at sensor height, and H is sensible heat flux (W/m²). Vapor pressure at the canopy surface e_0 (Pa) is given by:

$$e_0 = e_a + \frac{\lambda E \gamma}{\rho G_a c_p} \tag{8}$$

where e_a is air vapor pressure (Pa). VPD at the canopy surface (D_0) is given by Equations (7) and (8):

$$D_0 = E_{sat}(T_0) - e_0 \tag{9}$$

where $E_{sat}(T_0)$ is the saturation vapor pressure at temperature T_0. Likewise, CO_2 concentration at the canopy surface (C_0) can be approximated by:

$$C_0 = C_a + \frac{NEE}{G_a} \tag{10}$$

where G_a is for CO_2 and in mol m⁻² s⁻¹.

G_1 (Equation 3) was recalculated with D_a and C_a at measurement height replaced by their equivalents at the canopy surface (D_0 and

C_0, respectively), as given by Equations (9) and (10). Note that the calculated G_s (Equation 2) remains unchanged as the PM equation already accounts for meteorological deviations between the surface and measurement height.

2.3.4 | Energy balance closure

The PM equation that is inverted to estimate G_s (Equation 2) in this study assumes that the energy balance at the land surface is closed, i.e.:

$$A = R_n - G - S = H + \lambda E \tag{11}$$

where A is the available energy, R_n is the net radiation, G is the ground heat flux, S is the sum of all ecosystem storage terms (see, e.g., Leuning et al., 2012), λE is the latent heat flux, and H is the sensible heat flux (all in W/m²). A common issue observed for EC data is that the energy balance is not closed, as the turbulent fluxes (right part of Equation 11) typically do not sum up to the available energy. We tested the sensitivity of an unclosed energy balance to estimates of G_s derived from the PM equation and the corresponding G_1 considering three hypothetical extreme cases which differ with respect to the attribution of the residual of the energy balance closure (residual = $A - (H + \lambda E)$):

1. All error in H (denoted as $G_{s,H}$; $G_{1,H}$): Both A and λE are assumed to be correctly measured, and the residual is entirely ascribed to H. This case is implied by the PM equation (Equation 2).
2. All error in λE ($G_{s,\lambda E}$; $G_{1,\lambda E}$): Both A and H are assumed to be correctly measured, and the residual is entirely ascribed to λE, i.e., λE is recalculated as $\lambda E = A - H$.
3. All error in A ($G_{s,A}$; $G_{1,A}$): The turbulent fluxes H and λE are assumed to be correctly measured, and the energy imbalance is caused by an overestimation of A as a result of missing or inappropriate measurements of G and/or the components of S (i.e., $A = \lambda E + H$).

For comparison, G_s was additionally calculated using λE adjusted according to the Bowen ratio method (Twine et al., 2000), which assumes that the residual of the energy balance is attributed to H and λE according to the Bowen ratio ($H/\lambda E$; see http://fluxnet.fluxdata.org/data/fluxnet2015-dataset/data-processing/ for details on the calculation). Note that this approach, in contrast to the three cases considered above, does not force the energy balance to be closed at the sub-diurnal timescale.

The degree of the energy balance non-closure was quantified as the energy balance ratio (EBR):

$$EBR = \frac{\sum(H + \lambda E)}{\sum(R_n - G - S)} \tag{12}$$

where the individual energy balance components are either half-hourly/hourly values or summed up over a specified time period.

2.3.5 | NEE partitioning

The eddy covariance technique measures the NEE of CO_2 between the ecosystem and the atmosphere, but not its component fluxes GPP and ecosystem respiration (R_{eco}), which have to be estimated using flux partitioning algorithms. These algorithms, described below, can be classified into two main approaches: one that extrapolates nighttime NEE data to daytime, and one that fits light response curves to daytime NEE measurements. We calculate G_1 (Equation 3) using GPP derived from both approaches to assess the uncertainty in G_1 arising from uncertainties in the GPP estimates. The nighttime data-based approach (Reichstein et al., 2005) (denoted as GPP_{nt}; $G_{1,nt}$) relies on the use of a temperature response function fitted to nighttime NEE ($=R_{eco}$), which is then extrapolated to daytime conditions. The temperature response function (based on air temperature; Lloyd & Taylor, 1994) considers a time-varying base respiration, which implicitly accounts for additional environmental factors affecting R_{eco}. The daytime data-based approach (Lasslop et al., 2010) (GPP_{dt}; $G_{1,dt}$) fits a hyperbolic light response curve to daytime NEE. The function additionally accounts for temperature effects on R_{eco} and for VPD effects on GPP. We compared values of $G_{1,nt}$ and $G_{1,dt}$.

2.3.6 | Within-canopy gradients

Gradients of g_1 within the canopy cannot be directly inferred from eddy covariance data. Instead, the g_1 gradients were assessed with an integrative approach using both the EC data and a simple canopy model. The model simulates radiative transfer separately for sunlit and shaded fractions of the canopy (Spitters, 1986), which is separated into three vertical layers. Stomatal conductance and photosynthesis are modeled according to Equation (1) (Medlyn et al., 2011) and Farquhar, von Caemmerer, and Berry (1980) for each layer and are upscaled to the canopy level with the leaf area index (LAI). The model simulations were used to calculate the relative contribution of G_c from each layer to the total G_c. This fraction was considered as a proxy of the fraction of the G_1 signal coming from a certain layer (e.g., if G_c of the lowest layer contributed 20% to the total G_c, its contribution to the derived G_1 value was also assumed 20%). The EC data were then binned according to the relative contribution of G_c, and G_1 was estimated for each bin using Equation (3). Thus, the sun–shade radiation model served only to estimate the relative contribution of each canopy layer to G_c, whereas G_1 was directly estimated from the EC data and not from the modeled fluxes. Conditions where λE exceeded A were excluded. A random forest model (see Supporting Information) was used to explain the response of G_1 to the contribution of the respective canopy layer as well as other variables. Subsequently, the marginal effect of the contribution of the respective layer on G_1 was calculated, and a linear regression model was fitted to the resulting partial dependence function. An extrapolation of this linear regression fit to 1 gave an estimate of the corresponding G_1 value of the layer. The estimated within-canopy gradients were then compared to the estimated g_1 from leaf-level measurements made at different levels in the canopy for the sites DK-Sor and US-Ha1.

3 | RESULTS

Figure 1 shows time series of G_1 for the EC sites considered in this study as well as available leaf-level estimates of g_1 collected at the same location. The two estimates show a relatively good agreement for AU-Tum, but different magnitudes at the other sites, where both lower (GF-Guy, US-Ha1) and higher (FI-Hyy, FR-Pue) estimates were estimated from EC data. Ecosystem-level G_1 values were robust against alternative data filters with respect to the applied growing season and radiation thresholds (Fig. S4), but showed high interannual variability which could not be attributed to a single cause. In the following sections, we present the potential effects of different factors possibly contributing to the mismatch between the estimates from the two different data sources.

3.1 | Non-transpirational water fluxes

G_1 calculated with successively longer time periods after the last rainfall event removed (Figure 2) showed the steepest decrease in the first hours after rain followed by a more moderate decline for all sites except US-Ha1. This pattern is likely to reflect the decreasing fraction of soil and interception evaporation on ET with time after rainfall, which is associated with a decrease of nonphysiological contributions to the inferred G_s (Equation 2). Similar effects are expected from dew evaporation. However, the removal of time periods that are likely to be affected by dew evaporation did not result in noticeable changes in the G_1 estimates (Fig. S5). The calculated G_1 still shows a significant decrease after 3 days for some sites (e.g., 9% for FR-Pue, 19% for DK-Sor), which suggests a significant contribution of sustained soil evaporation. However, there is no clear relationship between the sensitivity of G_1 to the excluded time period after rainfall events and the LAI of the ecosystem, which indicates that the ongoing decline in G_1 is not driven solely by soil evaporation. Data several days after the last rainfall might, in addition, be affected by the onset of drought stress, albeit the most severe drought conditions are filtered out by the GPP-based growing season filter (Fig. S1).

3.2 | Aerodynamic conductance

The different G_a formulations (Equations 4–6; Fig. S6) inserted into the inverted PM equation (Equation 2) resulted in similar G_1 estimates, except for the formulation where G_a was assumed infinite ($G_{a,fcoupled}$; Equation 4) (Figure 3). The fully coupled assumption significantly overestimates G_s (Fig. S7a) and consequently G_1 (Figure 3a) for all site years. Compared to the reference formulation ($G_{a,empGb}$; Equation 5), the overestimation of G_1 resulting from neglecting G_a varied between 17% and 80% (site averages; mean of 50% over all site years) and depended not only on the magnitude of G_a but also
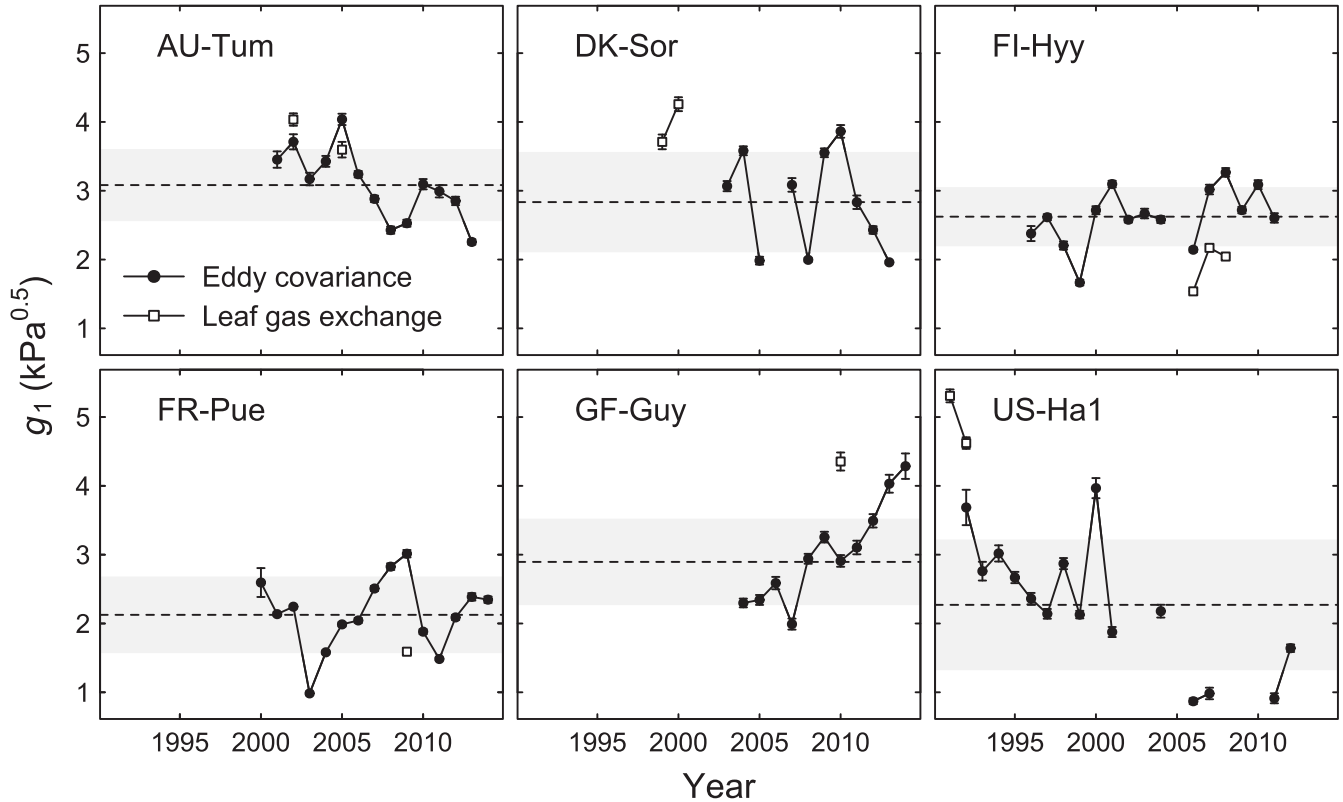
FIGURE 1 Time series of annual estimates of G_1 from eddy covariance (EC) data (filled circles) and g_1 from leaf gas exchange data taken at the top third of the canopy (open squares). For the EC data, G_1 was calculated using the following settings: 48 hr after rainfall removed, G_a calculated from Equation (5) ($G_{a,empGb}$), surface conditions, and $G_{1,H}$. Error bars indicate standard errors, dashed lines the mean across all years, and gray shaded areas the standard deviation of all annual G_1 values

on the evaporative fraction ($\lambda E/R_n$; Fig. S8) (Raupach & Finnigan, 1988). The $G_{a,physGb}$ model gave similar results for G_1 than the simpler $G_{a,empGb}$ formulation. The two estimates did not differ by more than 10% for 90% of all site years. Differences between $G_{a,empGb}$ and $G_{a,physGb}$ resulted solely from the boundary layer part (R_b, second term in Equations 5 and 6), which depends only on u_* in the empirical formulation ($G_{a,empGb}$), whereas it is affected by various

additional aerodynamic properties in the physically based model ($G_{a,physGb}$). In both formulations, R_b accounts for one-third to more than one half of the total aerodynamic resistance (Table S1). The $G_{a,physGb}$ model tends to predict lower G_a for broad-leaved vegetation (e.g., DK-Sor, GF-Guy) which reflects the formation of a thicker boundary layer around larger leaves (Fig. S6). The strong dependence of G_a on the leaf characteristic dimension (D_l) in this formulation (see
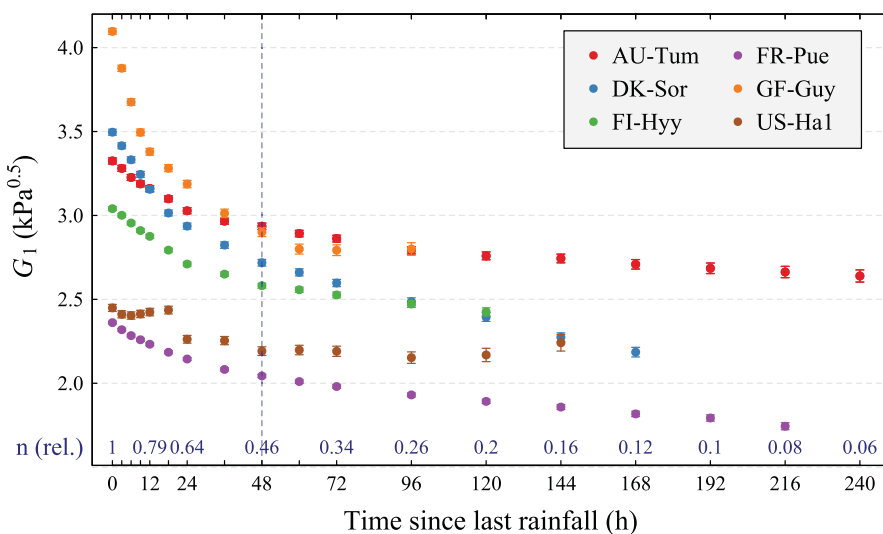
FIGURE 2 G_1 calculated excluding successively longer time periods after the last rainfall event removed (time since rainfall is considered as a proxy for the contribution of physical evaporation on ET). G_1 is only shown if the number of data exceeds 10% of all filtered data. n (rel.) denotes the relative amount of remaining data compared to no filter applied. The dashed blue line indicates the rainfall filter as applied in this study (48 hr). Error bars indicate standard errors

FIGURE 3 Mean annual G_1 estimated (Equation 3) with different calculation methods of aerodynamic conductance (G_a) used for the calculation of surface conductance (G_s; Equation 2). Estimated G_1 using G_a estimated from wind speed and friction velocity and an empirical canopy boundary layer conductance (G_b) model ($G_{a,empGb}$; Equation 5) is compared to (a) the fully coupled case ($G_{a,fcoupled}$; Equation 4) and (b) a physically based G_b formulation ($G_{a,physGb}$; Equation 6). Blue lines indicate reduced major axis (RMA) regression fits. Error bars indicate standard errors
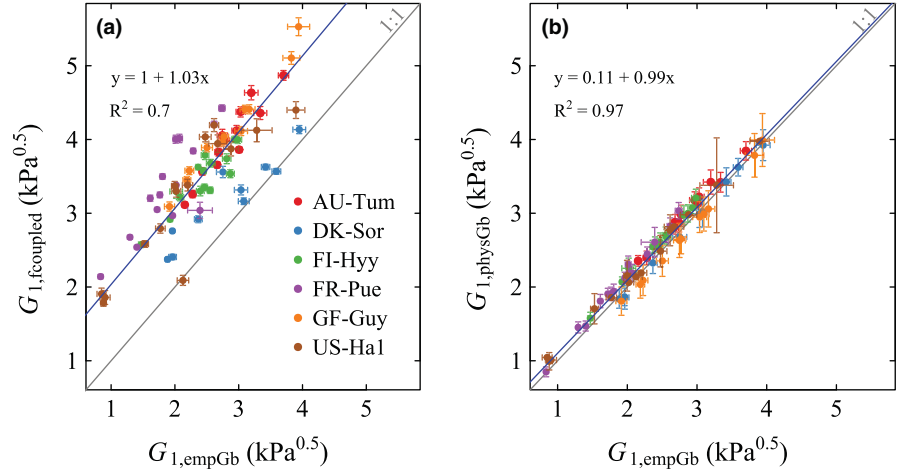
Equations S7 and S8) is associated with large uncertainties in G_a that propagate to G_s (Fig. S7b) and G_1. Assuming a standard deviation of 25% of the average D_l resulted in uncertainties in G_1 that mostly encompassed the G_1 values calculated using the empirical $G_{a,empGb}$ formulation (Figure 3b).
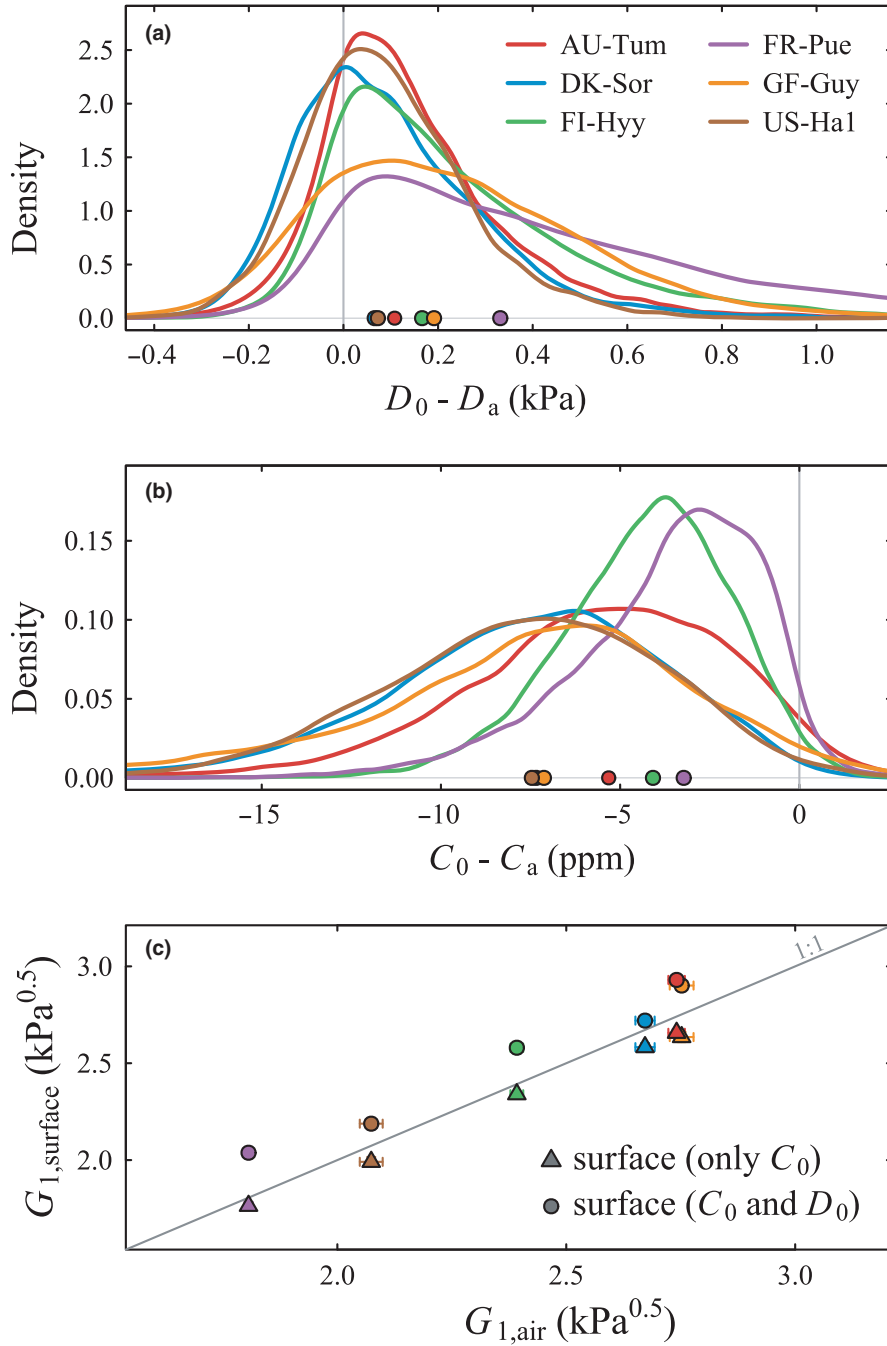
3.3 | Surface conditions

The inferred canopy surface conditions from the inverted bulk transfer equations for λE and H (Equations 7–9 using $G_{a,empGb}$ (Equation 5)) indicate that the canopy surface is in most conditions warmer (median c. 2°C) and more humid (median c. 0.1 kPa) than the air at measurement height (Fig. S9a,b). The temperature effect on VPD through an increase in E_{sat} was stronger than the effect of an increase in humidity, resulting in a mostly higher VPD (median c. 0.1–0.2 kPa) at the vegetation surface compared to the air above ($D_0 > D_a$; Figures 4a and S9c). Based on the theory elaborated by Jarvis and McNaughton (1986), Magnani, Leonardi, Tognetti, Grace, and Borghetti (1998) have shown that the difference between D_0 and D_a can be expressed as a rather complex function of the relative importance of imposed and equilibrium ET, the degree of canopy-atmosphere decoupling, and G_c. In general, the deviations are expected to be large when the degree of decoupling is high, G_c is low, and the difference of equilibrium and imposed ET is large (Magnani et al., 1998). The predominantly high deviations found for FR-Pue, for instance, can be linked to the low G_c relative to the other sites. The inferred molar concentration of CO_2 at the canopy surface (C_0) was lower than that in the air (C_a) as a consequence of vegetation uptake. The effect varied among sites depending on GPP and G_a (Equation 10), and typically ranged between 0 and 15 ppm.

The estimated G_1 using C_0 (Equation 3) was only marginally lower than the original estimate using C_a (2%–4%; Figure 4c). Replacing D_a in Equation (3) with D_0 had the opposite effect and led to slightly higher G_1 estimates, but the effect was again small (5%–15%). Owing to their minor and opposite effects on G_1, the substitution of both D_a and C_a with their analogs at the canopy surface D_0 and C_0 in Equation (3) resulted in marginal increases in G_1 (2%–13%; Figure 4c).

3.4 | Energy balance

Figure 5a–c depicts mean diurnal courses of the measured energy balance components for the three sites FI-Hyy, AU-Tum, and FR-Pue. The available energy A, represented by $A = R_n - G$ (black line), almost always exceeds the sum of the turbulent energy fluxes ($H + \lambda E$; green line), indicating a non-closed energy balance. The degree of closure of the energy balance was represented by the energy balance ratio (EBR, Equation 12; orange line). The deviation from a closed energy balance (i.e., the difference between A and $H + \lambda E$ or the residual of the energy balance closure, respectively) varied among sites. The mean EBR amounts to 0.83, 0.85, and 0.68 for FI-Hyy, AU-Tum, and FR-Pue, respectively, and is thus in the range of previously reported average values for the FLUXNET network (Stoy et al., 2013; Wilson et al., 2002). The diurnal course of the EBR changed markedly throughout the day for all sites but in a different manner. FI-Hyy and AU-Tum showed a consistent increase in the EBR from the morning to the evening with the energy balance being closed in the late afternoon and evening hours (EBR ~ 1). This pattern is characteristic for FLUXNET sites (Wilson et al., 2002). FR-Pue, in contrast, showed the opposite pattern and a mostly decreasing EBR throughout the day.

The fact that the EBR is smaller than 1 for most conditions has consequences for G_s inferred from the inverted PM equation (Equation 2), as this equation was derived under the assumption of a closed energy balance. The error associated with the inferred G_s depends on which components of the surface energy balance (Equation 11) are inadequately measured or (not) accounted for. Assigning the residual entirely to either H, λE, or A served to assess the maximum uncertainty in G_s arising from a non-closed energy balance. The assumption that the energy balance non-closure is completely a result of an underestimate of H ("all error in H" case), as implicitly assumed by the PM equation, consistently led to the lowest G_s values in case of an EBR < 1. Assigning the residual energy entirely to A by recalculating it as $A = H + \lambda E$ gives slightly higher estimates compared to the first case. By contrast, assuming that all the error is in λE (i.e., λE recalculated as $\lambda E = A - H$) yields significantly higher G_s estimates, reaching more than 100% overestimation compared to

FIGURE 4 Difference between inferred canopy surface conditions and measurements above the canopy for (a) vapor pressure deficit (*D*) and (b) CO_2 concentration (*C*), as well as (c) the resulting effects on G_1. Canopy surface *D* (D_0) was calculated from the inverted bulk transfer relations of latent and sensible heat flux (Equations 7–9), and the CO_2 concentration at the canopy surface (C_0) was calculated from measured net ecosystem exchange (Equation 10). For all calculations, G_a from Equation (5) was used. The filled circles in (a) and (b) indicate the medians of the distribution functions. G_1 in (c) represents the site mean over all available years (error bars indicate standard errors)

the reference case (all error in *H*) for all three sites. The difference between the G_s estimates from the three cases scales with the EBR. These three G_s estimates are identical if EBR = 1 and deviate for both lower and higher EBR values. The "Bowen ratio adjusted" case shows intermediate G_s values for most conditions but it may give higher G_s and G_1 values as the "all error in λE" case, as it does not force the energy balance to be closed on the sub-diurnal timescale. Importantly, diurnal variations in the EBR as found for all three sites affect the temporal behavior of G_s throughout the day (Figure 5d–f).

The uncertainty in G_s due to the non-closure of the energy balance propagates to the uncertainty in G_1, which shows a similar behavior as G_s and the highest values if the residual is attributed to

λE (Figure 5g–i). G_1 shows an even higher sensitivity to the EBR. This can be explained by the fact that the estimated G_1, in addition to G_s, responds to VPD and C_a, whose diurnal courses amplify the response of G_1 to the EBR (Equation 3). Importantly, not only the magnitude of G_1 but also its diurnal course is affected. For instance, G_1 at FI-Hyy and AU-Tum show a steady decrease if the residual is assigned to λE, but constant or slightly increasing values through most parts of the day if it is assigned to *H* or *A* (Figure 5g,h).

The sensitivity of G_s to an unclosed energy balance as quantified by the EBR (Equation 12) is illustrated in Figure 6. There is a high variability of the half-hourly EBR at each site, though most of the data are characterized by an EBR between 0.5 and 1.2, depending
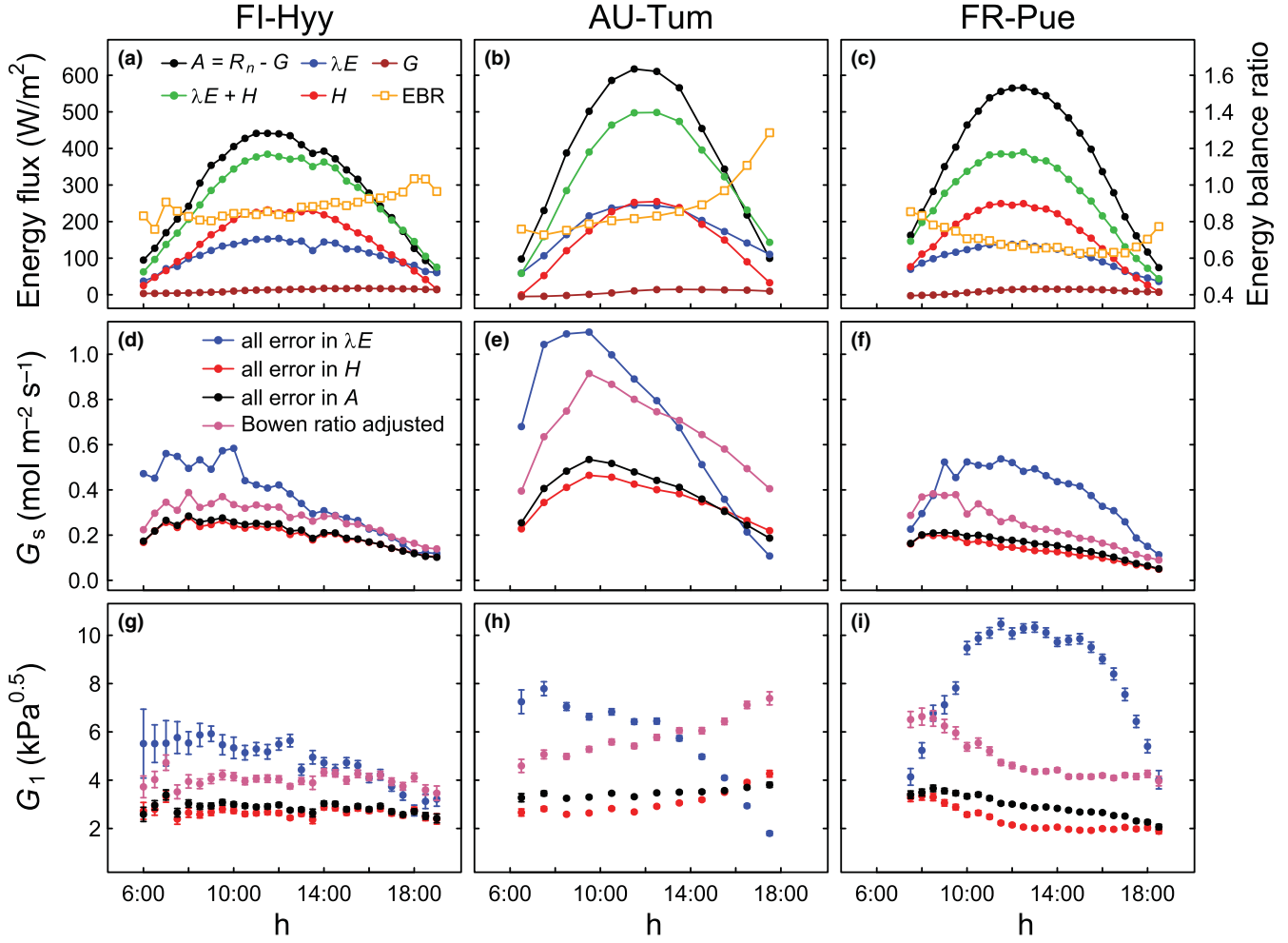
FIGURE 5 Mean diurnal courses (over all available site years) of (a–c) energy balance components and the energy balance ratio (EBR), (d–f) surface conductance (G_s), and (g–i) the corresponding G_1 for the sites FI-Hyy, AU-Tum, and FR-Pue. G_s was calculated from Equation (2) for three hypothetical extreme cases with respect to the attribution of the residual of the energy balance closure to either H, λE, or A, as well as for the Bowen ratio adjusted case. G_1 was estimated for all data in the respective half-hourly/hourly bin (Equation 3). Error bars indicate standard errors

on the time of day (Figure 5a–c) and most likely other conditions (e.g., turbulence intensity, Wilson et al., 2002; Leuning et al., 2012). The y-axis shows the ratio of the two most extreme estimates of G_s, which are given by $G_{s,\lambda E}$ (i.e., G_s calculated from Equation (2) assuming that the residual is entirely attributed to λE, i.e., $\lambda E = R_n (-G) - H$) and $G_{s,H}$ (i.e., assuming that the residual is entirely attributed to H). $G_{s,\lambda E}$ and $G_{s,H}$ are identical in case of a closed energy balance and yield the highest and lowest G_s estimates if the EBR < 1 and vice versa if the EBR > 1. Any deviation in the EBR from 1 (positive or negative) causes the ratio of the two extreme estimates of G_s to change exponentially with the EBR. The sensitivity of $G_{s,\lambda E}/G_{s,H}$ to the EBR is similar for all sites (fitted lines in Figure 6b) and varies only slightly with VPD and other variables (results not shown). A typical value of $G_{s,\lambda E}/G_{s,H}$ is c. 2 for sites with an average EBR of c. 0.8 (as, for example, in FI-Hyy) and exceeds 3 for sites with a poor energy balance closure (as, e.g., FR-Pue). It has to be noted that the ratio $G_{s,\lambda E}/G_{s,H}$ represents the maximum uncertainty in G_s. This uncertainty is considerably lower if the residual is to large parts the result of an overestimation of A. The "true" G_s and G_1 will most

likely not reach the two extreme cases $G_{s,\lambda E}$ and $G_{s,H}$, but lie somewhere in between. Their exact values can only be determined if the values of A, λE, and H are correctly known.

3.5 | NEE partitioning algorithm

The two algorithms ("daytime" (dt) and "nighttime" (nt)) that were used to partition NEE into its component fluxes GPP and R_{eco} yielded similar average GPP values for the filtered daytime data within the growing season ($R^2 = 0.97$; Figure 7a). Depending on the year, the nighttime method gave either higher or lower GPP estimates than the daytime method. Over all years, there was no consistent difference between the two methods across sites, but the nighttime approach tended to estimate higher GPP averages than the daytime method (Figure 7a). The patterns in GPP are clearly reflected in the G_1 values calculated using the two different GPP versions (Figure 7b). Higher estimates in GPP generally result in lower estimates of G_1 and vice versa. G_1 was further found to be relatively sensitive to GPP. On average, a change in GPP of
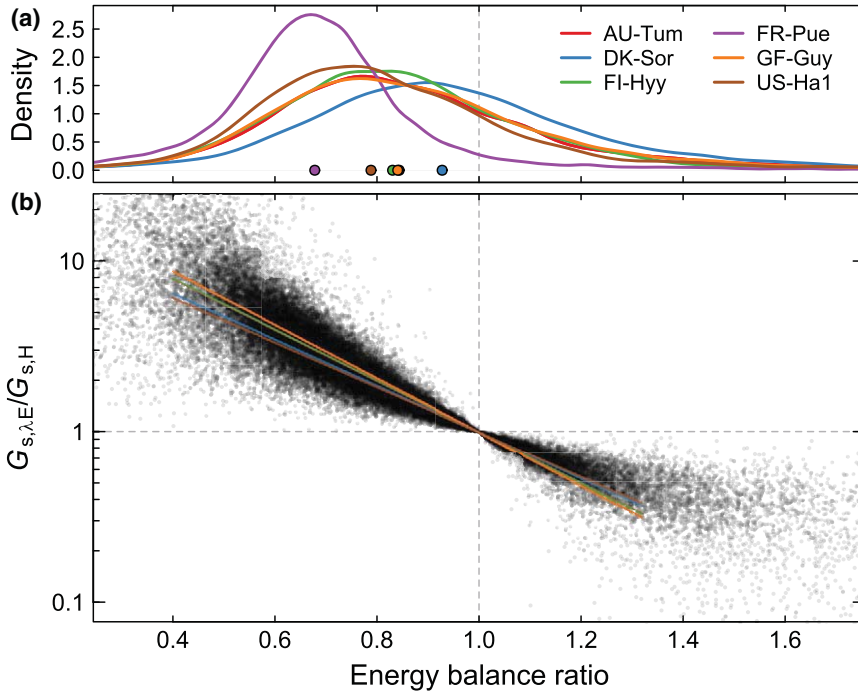
FIGURE 6 (a) Distribution of the half-hourly/hourly energy balance ratio (Equation 12) and (b) the maximum uncertainty in G_s (derived from the Penman–Monteith equation) resulting from an unclosed energy balance. The points in (a) indicate the median of the energy balance ratio. $G_{s,\lambda E}$ and $G_{s,H}$ in (b) are calculated from Equation (2) with $\lambda E = R_n - G - H$ (or $\lambda E = R_n - H$ if G is unavailable) and λE as measured from the eddy covariance data, respectively. Lines in (b) are fitted with weighted least squares regression
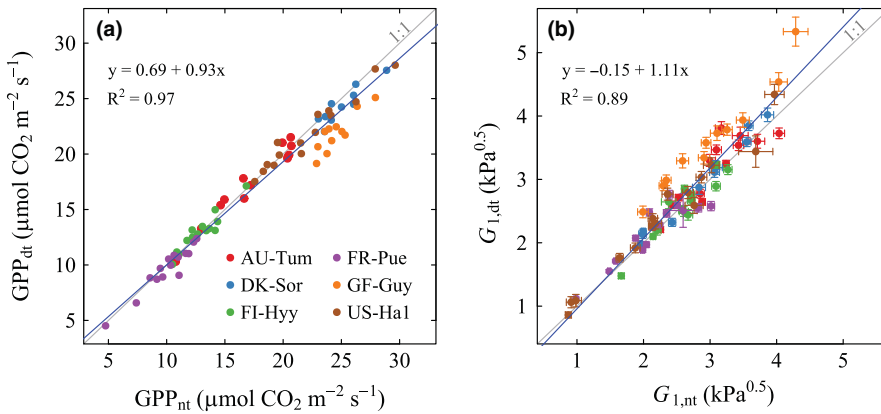

FIGURE 7 Estimates of (a) mean growing season gross primary productivity (GPP) and (b) G_1 (Equation 3) with GPP derived from a daytime (dt; Lasslop et al., 2010) and nighttime (nt; Reichstein et al., 2005) partitioning approach of net ecosystem exchange (NEE). Data are filtered as described in Materials and methods. Blue lines indicate reduced major axis (RMA) regression fits

1 μmol m^{-2} s^{-1} led to a change of 0.2 kPa$^{0.5}$ in G_1 across sites (Fig. S10).

3.6 | Within-canopy gradients

The partial dependence plots in Figure 8 display the marginal effects of the relative contributions of the top and bottom layer ($G_{c,layer}$/$G_{c,total}$; x-axis) on the ecosystem-level G_1 as estimated from the EC data (y-axis). All subplots (except Figure 8d (FR-Pue)) indicate that the contribution of the bottom layer G_c to the total G_c (black lines) increases along with the estimated G_1. In other words, under conditions when a comparatively large proportion of the G_1 signal comes from the lowest 1/3 of the canopy, G_1 as estimated from the EC data (Equation 3) tends to be higher than when the lowest layer's contribution is small. As expected, the pattern is reverted for the contribution of the top layer (blue lines), in which case an increase in the relative contribution of the top layer is associated with a decrease in G_1. The two marginal effects are consistent across sites in that they

imply higher G_1 values at the canopy bottom compared to the top, a behavior that is present at all sites except FR-Pue. An estimate of the within-canopy gradient was further made by fitting a linear model to the partial dependence plots, and extrapolating the fitted line to 1, the hypothetical value at which the entire G_1 signal comes from the respective layer (dots in Figure 8). The ratio of the two values (representing the G_1 value of the bottom and top layer, respectively) is then an indication of the gradient within the canopy (denoted as "Ratio" in Figure 8). The gradients differed from site to site. We found a moderately high correlation ($r = .76$) between the implied gradients and the degree of aerodynamic vegetation-atmosphere decoupling (results not shown). This may be an indication that relatively poorly coupled forests with tall and dense canopies (e.g., GF-Guy) are associated with higher within-canopy gradients. However, the low number of sites included in this study did not allow to investigate this aspect in more detail. The approach is further strongly affected by the effects of the energy balance non-closure on G_1, which are exceptionally critical for half-hourly/hourly data as used here (see Figure 5). At leaf
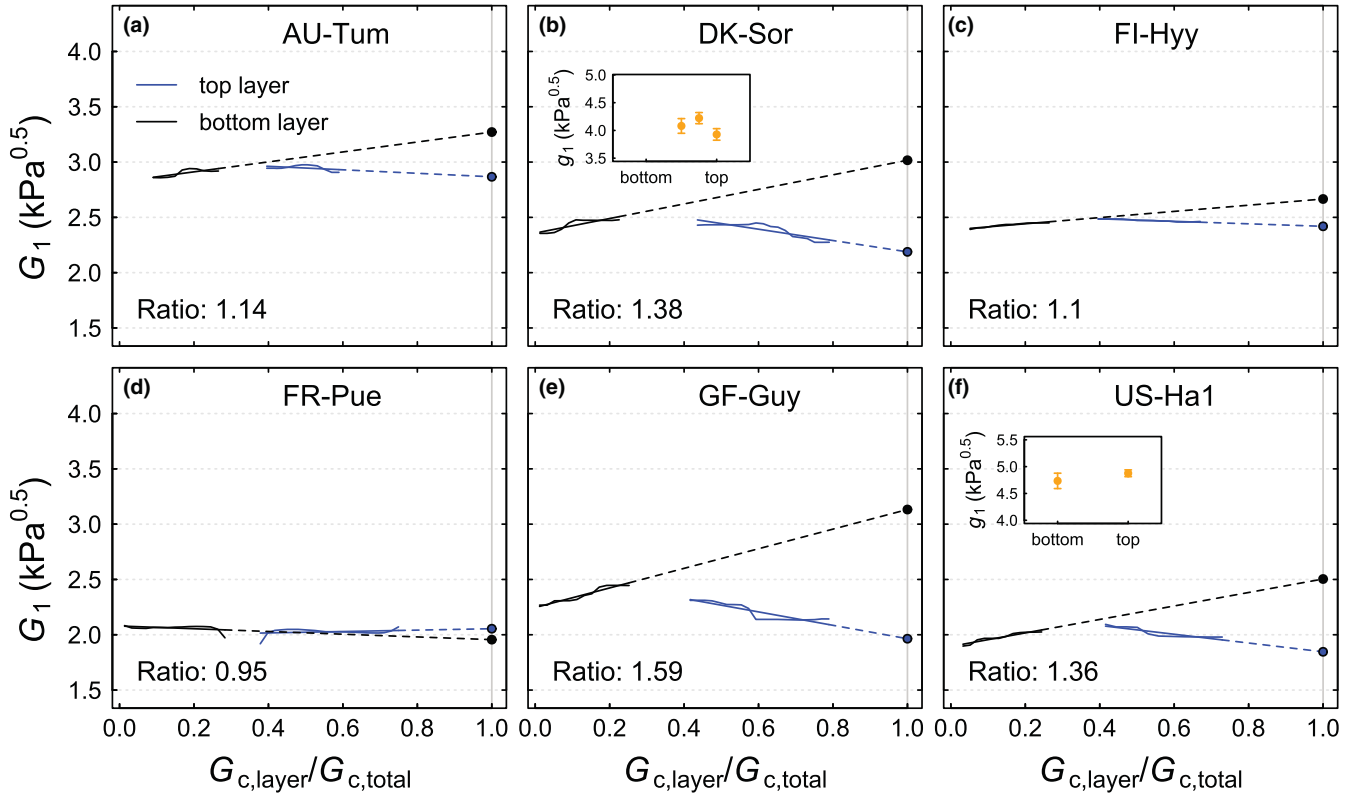
FIGURE 8 Partial dependence plots (solid lines) of the contribution of the top (blue line) and bottom layer (black line) (approximated as $G_{c,layer}/G_{c,total}$) on the estimated G_1 (Equation 3). The straight lines represent the ordinary least squares fit to the partial dependences (solid) and their extrapolation to 1 (dashed). The ratio of the extrapolated values at 1 (i.e., $G_{1,bottom}/G_{1,top}$) is indicated at the bottom left of each panel. Conditions where $\lambda E > A$ were excluded. Insets show g_1 estimates from available leaf gas exchange data at different positions in the canopy

level, g_1 estimates from different levels in the canopy did not indicate gradients at DK-Sor and US-Ha1 (insets in Figure 8b,f). It is important to note that G_1 gradients within the canopy can result from vertical gradients within plants of the same species or physiological differences between overstory and understory vegetation, information that can only be resolved with a more detailed knowledge on the vegetation at the site.

4 | DISCUSSION

In this study, we show that values of G_c and the intrinsic WUE metric G_1 inferred from EC data are affected by confounding physical factors and methodological uncertainties (Table 2). We demonstrated that factors that are often overlooked in an ecophysiological context (e.g., energy balance non-closure, aerodynamic conductance) can be more critical for the accurate estimation of WUE than factors which are more commonly acknowledged (e.g., NEE partitioning algorithm, soil evaporation). The fact that observed discrepancies between the two data sources (Figure 1) could not be fully resolved may be attributed to the low level of scientific understanding (and corresponding high uncertainty) of the factors considered here (Table 2), or to issues of representativeness in the sense that species contributing to the ecosystem fluxes are not sampled in the same proportion at the leaf level (Table 1).

TABLE 2 Effects of the factors investigated in this study on the derived ecosystem-level intrinsic water-use efficiency measure G_1 and their uncertainties

Factor	Impact on G_1 (%)		Uncertainty of the effect
(1) Interception and soil evaporation	Medium	−10 to 50	Medium-High
(2) Aerodynamic conductance	Medium-High	−10 to 70	Low
(3) Meteorological gradients canopy-air	Low	+0 to 15	Medium
(4) Energy balance non-closure	High	+0 to 400	High
(5) NEE partitioning	Low	±0 to 20	Medium
(6) Within-canopy gradients in g_1[a]	Low	−0 to 20	High

[a]Numbers refer to the canopy-integrated estimate of G_1 relative to g_1 from the top third of the canopy only (as measured by leaf gas exchange).

4.1 | Non-transpirational water fluxes

The physiological interpretation of G_s is compromised if measured λE comprises substantial non-transpirational contributions from the soil or canopy interception, in which case $G_s \gg G_c$ (Kelliher, Leuning, Raupach, & Schulze, 1995; Paw & Meyers, 1989). The effects of

non-transitional λE on G_s can be assessed by either extrapolating G_s from dry periods to rainfall periods (e.g., Knohl & Buchmann, 2005), or by excluding time periods following rainfall events, as was done here. Our results (Figure 2) underline the need to exclude time periods following precipitation in order to avoid an overestimation of G_c and thus G_1. An additional exclusion of time periods affected by dew evaporation was found not to be necessary for the sites studied here, possibly because the overall contribution of dew to the total evapotranspiration is minor (see, e.g., Jacobs, Heusinkveld, Wichink Kruit, & Berkowicz, 2006), or because the radiation threshold used here (200 μmol m^{-2} s^{-1}) was sufficient to exclude major dew evaporation fluxes. Our Results confirm previous approaches in which the excluded time period is restricted to 2 days after rainfall (e.g., Beer et al., 2009; Ponton et al., 2006), a practical approach with regard to the tradeoff between physiologically meaningful G_s estimates and a sufficient amount of data.

4.2 | Aerodynamic conductance and surface conditions

The effect of G_a on G_1 was found to be important for all ecosystems investigated here and is likely to be especially important for short-statured (poorly coupled) vegetation. Figure 3a demonstrates that the occasionally made assumption of a full aerodynamic coupling between the vegetation and the atmosphere (e.g., Beer et al., 2009; Groenendijk et al., 2011; Keenan et al., 2013) is, even for comparatively well coupled forests, not justified.

A simple estimate of G_a (Equation 5 or similar) is often embedded in the PM equation (e.g., Blanken & Black, 2004; Launiainen et al., 2016). This formulation only requires measurements of wind speed and u_* and gives values similar to more complex approaches (Figure 3b).

A major difficulty in the derivation of G_a at ecosystem level is the canopy boundary layer conductance (G_b) (e.g., Verhoef, De Bruin, & Van Den Hurk, 1997). Replacing the empirical G_b model (Equation 5) with a physically based formulation (Equation 6) (Massman, 1999; Su et al., 2001) considers a more comprehensive set of aerodynamically relevant properties of the ecosystem, but also introduces additional uncertainties. This is problematic due to the high sensitivity of this formulation (and that of others, e.g., McNaughton & Van den Hurk, 1995) to the characteristic leaf dimension (Equations S2, S7, and S8); Figure 3b), information that is not always available and presumably highly variable at EC sites.

Using G_a to infer the micrometeorology at the big-leaf surface as the physiologically relevant conditions (Grantz & Meinzer, 1990) resulted in better model fits (Table S2), but had minor effects on the mean growing season G_1 values for the ecosystems investigated here. It appears unlikely that G_1 will be significantly affected by meteorological gradients within the canopy, as they have often been found to be even less pronounced than those between canopy and tower height (Linderson et al., 2012; Schurgers, Lagergren, Mölder, & Lindroth, 2015). However, meteorological gradients are likely to be more relevant for more decoupled ecosystems (e.g., grasslands,

croplands) but this also strongly depends on site-specific micrometeorological conditions (Magnani et al., 1998).

4.3 | Energy balance closure

Energy balance non-closure, i.e., the phenomenon that the sum of the measured turbulent fluxes H and λE is smaller than the available energy, is observed at most EC sites (Stoy et al., 2013; Wilson et al., 2002). Potential reasons for this issue are manifold (Foken, 2008; Leuning et al., 2012), but involve either an underestimation of the turbulent fluxes by EC measurement systems (due to, e.g., low-frequency losses resulting from mesoscale circulations; Foken, 2008; Stoy et al., 2013) or an overestimation of A, which arises predominantly when energy storage terms (S) are neglected. Yet, not all components of S can be readily determined. For example, the energy storage flux into and out of the aboveground biomass, which can sum up to approximately half of S in forest ecosystems (Lindroth, Mölder, & Lagergren, 2010), has to be estimated from biomass temperature, mass of the aboveground biomass as well as its heat capacity (see, e.g., Haverd, Cuntz, Leuning, & Keith, 2007), information that is not available for most sites.

An unclosed energy balance affects the derivation of G_s from the inverted PM equation, since the latter assumes the energy balance to be closed. Our results demonstrate that the inferred G_s is sensitive to a violation of this assumption, in agreement with the analysis for a grassland and a shrub ecosystem by Wohlfahrt et al. (2009). The error in G_s that is made due to the energy balance non-closure depends on which component of the energy balance is misrepresented in the measurements. An important implication is that the PM equation (Equation 2) implicitly assigns the residual entirely to H and, therefore, underestimates (overestimates) G_s when the EBR < 1 (EBR > 1). G_s is less sensitive to errors in S, but highly sensitive to errors in λE, with potential errors rising exponentially with a decline in the EBR (Figure 6b). In addition, an often observed diurnal cycle in the EBR also affects the diurnal courses of G_s (Figure 5d–f). Thus, both the magnitude and the temporal dynamics of G_s are strongly confounded by (and dependent on) the degree of closure in the energy balance, which is problematic as the EBR is not expected to be a physiologically relevant driver of iWUE. The uncertainty in G_s propagates to G_1 (Figure 5), which further depends on to what extent carbon fluxes are affected by the energy balance closure problem (see Barr, Morgenstern, Black, McCaughey, & Nesic, 2006).

Our results call for accurate measurements of the surface energy storage terms (S in Equation 11) and their diurnal courses at EC sites. This information would help to constrain uncertainties in G_s and ultimately allow application of flux correction procedures (Twine et al., 2000; "Bowen ratio adjusted" case in Figure 5), which "overcorrect" half-hourly/hourly turbulent fluxes if S and/or G are neglected, particularly in ecosystems with tall vegetation and high biomass. Careful consideration of all energy balance terms (as, e.g., in Blanken et al., 1997; Barr et al., 2006; Jacobs, Heusinkveld, & Holtslag, 2008) and, where appropriate, adjustment of the turbulent

fluxes are crucial for the derivation and physiological interpretation of EC-derived gas exchange characteristics on a sub-daily time scale.

4.4 | NEE partitioning and uncertainties across scales

Figure 7 suggests that ecosystem-level G_1 is relatively robust to choices made on the partitioning approach, which is in line with the general good agreement between the two GPP products (Lasslop et al., 2010). Nonetheless, the high sensitivity of G_1 to GPP emphasizes the importance of correctly estimating GPP from EC data, which also relies on the use of a representative driving temperature for R_{eco} (Lasslop et al., 2012). Also relevant for the direct comparison of g_1 at leaf and ecosystem levels are differences in the carbon uptake term used in Equations (1) and (3): net photosynthesis (A_n) at the leaf level and GPP at the canopy level. The two have to be interpreted differently for two main reasons: (i) GPP estimated from flux partitioning algorithms integrates carboxylation (V_c) minus photorespiration (R_p) and is thus not equivalent to (and to some extent larger than) net photosynthesis ($A_n = V_c - R_p - R_L$) measured from leaf-level gas exchange. (ii) Leaf respiration in the dark (R_D) has been found to exceed that in daylight (R_L) (Atkin, Westbeek, Cambridge, Lambers, & Pons, 1997; Brooks & Farquhar, 1985), though a recent study suggests that this "Kok effect" could also be explained by changes in the chloroplastic CO_2 concentration (C_c) caused by a reduced mesophyll conductance at low light (Farquhar & Busch, 2017), in which case R_D would not necessarily be down-regulated in the light. The consequence of a larger R_D compared to R_L would be that an extrapolation of nighttime respiration to daytime overestimates GPP (Wohlfahrt & Gu, 2015). This effect is not considered in common flux partitioning approaches because it would require additional modeling efforts (e.g., light distribution within the canopy), knowledge of the fraction of leaf respiration to ecosystem respiration (Wohlfahrt, Bahn, Haslwanter, Newesely, & Cernusca, 2005), and because the inhibition effect (i.e., the ratio R_L/R_D) is not well constrained (Niinemets, 2014). Both these issues lead to a lower estimate of G_1 at the ecosystem level compared to the leaf level. Estimates of canopy-scale R_L from our simulations amount to 3.4% of GPP on average across sites, whereas overestimation of GPP due to a possible light inhibition of R_D would be in the order of 15% (Janssens et al., 2001; Wehr et al., 2016; Wohlfahrt et al., 2005), indicating that the latter is the more relevant source of disagreement between across-scale estimates of G_1, but clearly a better process understanding is needed (Farquhar & Busch, 2017).

4.5 | Within-canopy gradients

Pronounced canopy gradients of G_1 as estimated in this study for some sites (Figure 8) were not supported by leaf-level measurements at DK-Sor and US-Ha1. However, canopy gradients were in agreement with several observational studies reporting a lower iWUE (corresponding to a higher g_1) in the understory both across (Domingues, Martinelli, & Ehleringer, 2007) and within species (Sellin,

Eensalu, & Niglas, 2010), a pattern that results from the maintenance of a relatively high g_s at the canopy bottom compared to the top (Chazdon, 1988). As EC measurements integrate G_1 over the existing canopy gradients whereas leaf measurements do not, the former are expected to give higher values than the latter (if taken at the top of the canopy). This effect depends both on the gradient itself as well as the relative flux contribution from the different layers. Our results indicate that within-canopy gradients of g_1 are site- and possibly species-specific, highlighting the need for additional leaf-level measurements at different levels in the canopy, as well as a more comprehensive characterization of the understory vegetation and its contribution to total ecosystem fluxes.

4.6 | Recommendations for future studies

In this study, we aimed to derive a physiologically meaningful WUE metric (G_1) from EC data that can be used in modeling and for the characterization of the physiological control of ecosystem water–carbon coupling. We were limited to forest sites in this study by the availability of leaf gas exchange data, but it would be useful to extend this analysis to non-forest sites or to include carbon isotope data as an independent dataset (as, e.g., in Medlyn et al. (2017)). We demonstrate that EC-derived G_s and G_1 are strongly affected by (i) confounding physical factors and (ii) methodological uncertainties, and are subject to (iii) conceptual differences to leaf-level estimates. Ignoring these factors compromises the ecophysiological interpretation of EC-derived vegetation gas exchange characteristics as well as their direct comparison to leaf-level estimates. Based on our analysis, we have the following recommendations for the calculation of G_1:

- Exclusion of time periods for at least 24 hr after rainfall.
- The assumption $G_a = \infty$ is inappropriate; the use of physically based G_a models is only recommended if site-specific aerodynamic properties are known.
- The derivation of canopy surface meteorology (e.g., VPD) is meaningful, but of secondary importance for average growing season values.
- Critical evaluation and (if appropriate) correction of all energy balance terms is pivotal.
- Both daytime and nighttime NEE partitioning algorithms can be used for WUE studies.
- EC data should be complemented by physiological (leaf level) and meteorological measurements made at different levels in the canopy.

REFERENCES

Anderson, M. C., Kustas, W. P., & Norman, J. M. (2003). Upscaling and downscaling − A regional view of the soil-plant-atmosphere continuum. *Agronomy Journal*, *95*, 1408–1423.

Atkin, O. K., Westbeek, M. H., Cambridge, M. L., Lambers, H., & Pons, T. L. (1997). Leaf respiration in light and darkness (a comparison of slow-and fast-growing Poa species). *Plant Physiology*, *113*, 961–965.

Aubinet, M., Grelle, A., Ibrom, A., Rannik, Ü., Moncrieff, J., Foken, T., ... Vesala, T. (1999). Estimates of the annual net carbon and water exchange of forests: The EUROFLUX methodology. *Advances in Ecological Research*, *30*, 113–175.

Ball, J. T., Woodrow, I. E., & Berry, J. A. (1987). A model predicting stomatal conductance and its contribution to the control of photosynthesis under different environmental conditions. In J. Biggins (Ed.), *Progress in photosynthesis research* (pp. 221–224). Dordrecht, the Netherlands: Martinus Nijhoff Publishers.

Barnard, D., & Bauerle, W. (2013). The implications of minimum stomatal conductance on modeling water flux in forest canopies. *Journal of Geophysical Research: Biogeosciences*, *118*, 1322–1333.

Barr, A., Morgenstern, K., Black, T., McCaughey, J., & Nesic, Z. (2006). Surface energy balance closure by the eddy-covariance method above three boreal forest stands and implications for the measurement of the CO_2 flux. *Agricultural and Forest Meteorology*, *140*, 322–337.

Bassow, S., & Bazzaz, F. (1997). Intra-and inter-specific variation in canopy photosynthesis in a mixed deciduous forest. *Oecologia*, *109*, 507–515.

Beer, C., Ciais, P., Reichstein, M., Baldocchi, D., Law, B. E., Papale, D., ... Wohlfahrt, G. (2009). Temporal and among-site variability of inherent water use efficiency at the ecosystem level. *Global Biogeochemical Cycles*, *23*, GB2018.

Blanken, P., & Black, T. (2004). The canopy conductance of a boreal aspen forest, Prince Albert National Park, Canada. *Hydrological Processes*, *18*, 1561–1578.

Blanken, P., Black, T., Yang, P., Neumann, H. H., Nesic, Z., Staebler, R., ... Lee, X. (1997). Energy balance and canopy conductance of a boreal aspen forest: Partitioning overstory and understory components. *Journal of Geophysical Research*, *102*, 915–927.

Bonal, D., Bosc, A., Ponton, S., Baldocchi, D., Law, B. E., Papale, D., ... Wohlfahrt, G. (2008). Impact of severe dry season on net ecosystem exchange in the Neotropical rainforest of French Guiana. *Global Change Biology*, *14*, 1917–1933.

Brooks, A., & Farquhar, G. (1985). Effect of temperature on the CO_2/O_2 specificity of ribulose-1, 5-bisphosphate carboxylase/oxygenase and the rate of respiration in the light. *Planta*, *165*, 397–406.

Chazdon, R. L. (1988). Sunflecks and their importance to forest understorey plants. *Advances in Ecological Research*, *18*, 1–63.

de Pury, D., & Farquhar, G. (1997). Simple scaling of photosynthesis from leaves to canopies without the errors of big-leaf models. *Plant, Cell and Environment*, *20*, 537–557.

Denmead, O., Dunin, F., Wong, S., & Greenwood, E. (1993). Measuring water use efficiency of eucalypt trees with chambers and micrometeorological techniques. *Journal of Hydrology*, *150*, 649–664.

Desai, A. R., Richardson, A. D., Moffat, A. M., Kattge, J., Hollinger, D. Y., Barr, A., ... Stauch, V. J. (2008). Cross-site evaluation of eddy covariance GPP and RE decomposition techniques. *Agricultural and Forest Meteorology*, *148*, 821–838.

Domingues, T. F., Martinelli, L. A., & Ehleringer, J. R. (2007). Ecophysiological traits of plant functional groups in forest and pasture ecosystems from eastern Amazonia, Brazil. *Plant Ecology*, *193*, 101–112.

Dubbert, M., Piayda, A., Cuntz, M., Correia, A. C., Costa e Silva, F., Pereira, J. S., & Werner, C. (2014). Stable oxygen isotope and flux partitioning demonstrates understory of an oak savanna contributes up to half of ecosystem carbon and water exchange. *Frontiers in Plant Science*, *5*, 530.

Farquhar, G. D., & Busch, F. A. (2017). Changes in the chloroplastic CO_2 concentration explain much of the observed Kok effect: A model. *New Phytologist*, *214*, 570–584.

Farquhar, G., Hubick, K., Condon, A., & Richards, R. (1989). Carbon isotope fractionation and plant water-use efficiency. In P. Rundel, J. R. Ehleringer & K. Nagy (Eds.), *Stable isotopes in ecological research* (pp. 21–40). New York, NY: Springer.

Farquhar, G., von Caemmerer, S., & Berry, J. (1980). A biochemical model of photosynthetic CO_2 assimilation in leaves of C3 species. *Planta*, *149*, 78–90.

Foken, T. (2008). The energy balance closure problem: An overview. *Ecological Applications*, *18*, 1351–1367.

Grantz, D., & Meinzer, F. (1990). Stomatal response to humidity in a sugarcane field: Simultaneous porometric and micrometeorological measurements. *Plant, Cell and Environment*, *13*, 27–37.

Groenendijk, M., Dolman, A., Ammann, C., Arneth, A., Cescatti, A., Dragoni, D., ... Wohlfahrt, G. (2011). Seasonal variation of photosynthetic model parameters and leaf area index from global Fluxnet eddy covariance data. *Journal of Geophysical Research: Biogeosciences*, *116*, G04027.

Haverd, V., Cuntz, M., Leuning, R., & Keith, H. (2007). Air and biomass heat storage fluxes in a forest canopy: Calculation within a soil vegetation atmosphere transfer model. *Agricultural and Forest Meteorology*, *147*, 125–139.

Ito, A., & Inatomi, M. (2012). Water-use efficiency of the terrestrial biosphere: A model analysis focusing on interactions between the global carbon and water cycles. *Journal of Hydrometeorology*, *13*, 681–694.

Jacobs, A. F., Heusinkveld, B. G., & Holtslag, A. A. (2008). Towards closing the surface energy budget of a mid-latitude grassland. *Boundary-Layer Meteorology*, *126*, 125–136.

Jacobs, A. F., Heusinkveld, B. G., Wichink Kruit, R. J., & Berkowicz, S. M. (2006). Contribution of dew to the water budget of a grassland area in the Netherlands. *Water Resources Research*, *42*, 1–8.

Janssens, I., Lankreijer, H., Matteucci, G., Kowalski, A. S., Buchmann, N., Epron, D., ... Valentini, R. (2001). Productivity overshadows temperature in determining soil and ecosystem respiration across European forests. *Global Change Biology*, *7*, 269–278.

Jarvis, P. G., & McNaughton, K. (1986). Stomatal control of transpiration: Scaling up from leaf to region. *Advances in Ecological Research*, *15*, 1–49.

Keenan, T. F., Hollinger, D. Y., Bohrer, G., Dragoni, D., Munger, J. W., Schmid, H. P., & Richardson, A. D. (2013). Increase in forest water-use efficiency as atmospheric carbon dioxide concentrations rise. *Nature*, *499*, 324–327.

Kelliher, F., Leuning, R., Raupach, M., & Schulze, E.-D. (1995). Maximum conductances for evaporation from global vegetation types. *Agricultural and Forest Meteorology*, *73*, 1–16.

Kelliher, F., Lloyd, J., Arneth, A., Byers, J. N., McSeveny, T. M., Milukova, I., ... Schulze, E.-D. (1998). Evaporation from a central Siberian pine forest. *Journal of Hydrology*, *205*, 279–296.

Knauer, J., Zaehle, S., Reichstein, M., Medlyn, B. E., Forkel, M., Hagemann, S., & Werner, C. (2017). The response of ecosystem water-use efficiency to rising atmospheric CO_2 concentrations: sensitivity and large-scale biogeochemical implications. *New Phytologist*, *213*, 1654–1666.

Knohl, A., & Buchmann, N. (2005). Partitioning the net CO_2 flux of a deciduous forest into respiration and assimilation using stable carbon isotopes. *Global Biogeochemical Cycles*, *19*, GB4008.

Kolari, P., Lappalainen, H. K., Hänninen, H., & Hari, P. (2007). Relationship between temperature and the seasonal course of photosynthesis in Scots pine at northern timberline and in southern boreal zone. *Tellus Series B*, *59*, 542–552.

Lasslop, G., Migliavacca, M., Bohrer, G., Reichstein, M., Bahn, M., Ibrom, A., ... Cescatti, A. (2012). On the choice of the driving temperature for eddy-covariance carbon dioxide flux partitioning. *Biogeosciences*, *9*, 5243–5259.

Lasslop, G., Reichstein, M., Papale, D., Richardson, A. D., Arneth, A., Barr, A., ... Wohlfahrt, G. (2010). Separation of net ecosystem exchange into assimilation and respiration using a light response curve approach: Critical issues and global evaluation. *Global Change Biology*, *16*, 187–208.

Launiainen, S., Katul, G. G., Kolari, P., Vesala, T., & Hari, P. (2011). Empirical and optimal stomatal controls on leaf and ecosystem level CO_2 and H_2O exchange rates. *Agricultural and Forest Meteorology*, *151*, 1672–1689.

Launiainen, S., Katul, G. G., Kolari, P., Lindroth, A., Lohila, A., Aurela, M., ... Vesala, T. (2016). Do the energy fluxes and surface conductance of boreal coniferous forests in Europe scale with leaf area? *Global Change Biology*, *22*, 4096–4113.

Leuning, R. (1995). A critical appraisal of a combined stomatal-photosynthesis model for C3 plants. *Plant, Cell and Environment*, *18*, 339–355.

Leuning, R., Cleugh, H. A., Zegelin, S. J., & Hughes, D. (2005). Carbon and water fluxes over a temperate Eucalyptus forest and a tropical wet/dry savanna in Australia: Measurements and comparison with MODIS remote sensing estimates. *Agricultural and Forest Meteorology*, *129*, 151–173.

Leuning, R., Van Gorsel, E., Massman, W. J., & Isaac, P. R. (2012). Reflections on the surface energy imbalance problem. *Agricultural and Forest Meteorology*, *156*, 65–74.

Lin, Y.-S., Medlyn, B. E., Duursma, R. A., Prentice, I. C., Wang, H., Baig, S., ... Wingate, L. (2015). Optimal stomatal behaviour around the world. *Nature Climate Change*, *5*, 459–464.

Linderson, M.-L., Mikkelsen, T., Ibrom, A., Lindroth, A., Ro-Poulsen, H., & Pilegaard, K. (2012). Up-scaling of water use efficiency from leaf to canopy as based on leaf gas exchange relationships and the modeled in-canopy light distribution. *Agricultural and Forest Meteorology*, *152*, 201–211.

Lindroth, A., Mölder, M., & Lagergren, F. (2010). Heat storage in forest biomass improves energy balance closure. *Biogeosciences*, *7*, 301–313.

Lloyd, J., & Taylor, J. (1994). On the temperature dependence of soil respiration. *Functional Ecology*, *8*, 315–323.

Long, S., & Bernacchi, C. (2003). Gas exchange measurements, what can they tell us about the underlying limitations to photosynthesis? Procedures and sources of error. *Journal of Experimental Botany*, *54*, 2393–2401.

Maechler, M., Rousseeuw, P., Croux, C. Todorov, V., Ruckstuhl, A., Salibian-Barrera, M., ... di Palma, A. M. (2016). robustbase: Basic Robust Statistics R package version 0.92-7. URL http://CRAN.Rproject.org/package=robustbase.

Magnani, F., Leonardi, S., Tognetti, R., Grace, J., & Borghetti, M. (1998). Modelling the surface conductance of a broad-leaf canopy: Effects of partial decoupling from the atmosphere. *Plant, Cell and Environment*, *21*, 867–879.

Martin-StPaul, N. K., Limousin, J.-M., Rodríguez-Calcerrada, J., Ruffault, J., Rambal, S., Letts, M. G., & Misson, L. (2012). Photosynthetic sensitivity to drought varies among populations of *Quercus ilex* along a rainfall gradient. *Functional Plant Biology*, *39*, 25–37.

Massman, W. (1999). A model study of kB_H^{-1} for vegetated surfaces using 'localized near-field' Lagrangian theory. *Journal of Hydrology*, *223*, 27–43.

McNaughton, K., & Van den Hurk, B. (1995). A 'Lagrangian' revision of the resistors in the two-layer model for calculating the energy budget of a plant canopy. *Boundary-Layer Meteorology*, *74*, 261–288.

Medlyn, B. E., De Kauwe, M., Lin, Y.-S., Knauer, J., Duursma, R. A., Williams, C. A., ... Wingate, L. (2017). How do leaf and ecosystem measures of water-use efficiency compare? *New Phytologist*.

Medlyn, B. E., Duursma, R. A., Eamus, D., Ellsworth, D. S., Prentice, C. I., Barton, C. V. M., ... Wingate, L. (2011). Reconciling the optimal and empirical approaches to modelling stomatal conductance. *Global Change Biology*, *17*, 2134–2144.

Medlyn, B. E., Pepper, D. A., O'Grady, A. P., & Keith, H. (2007). Linking leaf and tree water use with an individual-tree model. *Tree Physiology*, *27*, 1687–1699.

Monteith, J. (1965). Evaporation and environment. In G. E. Fogg (Ed.), *The state and movement of water in living organisms* (pp. 205–234). Cambridge: Cambridge University Press 19th Symp. Soc. Exp. Biol.

Niinemets, Ü. (2014). Improving modeling of the 'dark part' of canopy carbon gain. *Tree Physiology*, *34*, 557–563.

Osmond, C., Björkman, O., & Anderson, D. (1980). *Physiological processes in plant ecology*. Berlin: Springer.

Papale, D., Reichstein, M., Aubinet, M., Canfora, E., Bernhofer, C., Kutsch, W., ... Yakir, D. (2006). Towards a standardized processing of Net Ecosystem Exchange measured with eddy covariance technique: algorithms and uncertainty estimation. *Biogeosciences*, *3*, 571–583.

Paw, U. K. T., & Meyers, T. P. (1989). Investigations with a higher-order canopy turbulence model into mean source-sink levels and bulk canopy resistances. *Agricultural and Forest Meteorology*, *47*, 259–271.

Pilegaard, K., Ibrom, A., Courtney, M. S., Hummelshøj, P., & Jensen, N. O. (2011). Increasing net CO_2 uptake by a Danish beech forest during the period from 1996 to 2009. *Agricultural and Forest Meteorology*, *151*, 934–946.

Ponton, S., Flanagan, L. B., Alstad, K. P., Johnson, B. G., Morgenstern, K., Kljun, N., ... Barr, A. G. (2006). Comparison of ecosystem water-use efficiency among Douglas-fir forest, aspen forest and grassland using eddy covariance and carbon isotope techniques. *Global Change Biology*, *12*, 294–310.

Rambal, S., Ourcival, J.-M., Joffre, R., Mouillot, F., Nouvellon, Y., Reichstein, M., & Rocheteau, A. (2003). Drought controls over conductance and assimilation of a Mediterranean evergreen ecosystem: Scaling from leaf to canopy. *Global Change Biology*, *9*, 1813–1824.

Raupach, M., & Finnigan, J. (1988). 'Single-layer models of evaporation from plant canopies are incorrect but useful, whereas multilayer models are correct but useless': Discuss. *Functional Plant Biology*, *15*, 705–716.

Reichstein, M., Bahn, M., Mahecha, M. D., Kattge, J., & Baldocchi, D. D. (2014). Linking plant and ecosystem functional biogeography. *Proceedings of the National Academy of Sciences*, *111*, 13697–13702.

Reichstein, M., Falge, E., Baldocchi, D., Papale, D., Valentini, R., Aubinet, M., ... Yakir, D. (2005). On the separation of net ecosystem exchange into assimilation and ecosystem respiration: Review and improved algorithm. *Global Change Biology*, *11*, 1424–1439.

Schulze, E.-D., & Hall, A. (1982). Stomatal responses, water loss and CO_2 assimilation rates of plants in contrasting environments. In O. Lange,

P. Nobel, C. Osmond & H. Ziegler (Eds.), *Physiological plant ecology II* (pp. 181–230). Berlin: Springer.

Schurgers, G., Lagergren, F., Mölder, M., & Lindroth, A. (2015). The importance of micrometeorological variations for photosynthesis and transpiration in a boreal coniferous forest. *Biogeosciences*, *12*, 237–256.

Sellin, A., Eensalu, E., & Niglas, A. (2010). Is distribution of hydraulic constraints within tree crowns reflected in photosynthetic water-use efficiency? An example of *Betula pendula*. *Ecological Research*, *25*, 173–183.

Shuttleworth, W. J., & Wallace, J. (1985). Evaporation from sparse crops-an energy combination theory. *Quarterly Journal of the Royal Meteorological Society*, *111*, 839–855.

Spitters, C. (1986). Separating the diffuse and direct component of global radiation and its implications for modeling canopy photosynthesis Part II. Calculation of canopy photosynthesis. *Agricultural and Forest Meteorology*, *38*, 231–242.

Stoy, P. C., Mauder, M., Foken, T., Marcolla, B., Boegh, E., Ibrom, A., ... Varlagin, A. (2013). A data-driven analysis of energy balance closure across FLUXNET research sites: The role of landscape scale heterogeneity. *Agricultural and Forest Meteorology*, *171*, 137–152.

Su, Z., Schmugge, T., Kustas, W., & Massman, W. (2001). An evaluation of two models for estimation of the roughness height for heat transfer between the land surface and the atmosphere. *Journal of Applied Meteorology*, *40*, 1933–1951.

Thom, A. (1972). Momentum, mass and heat exchange of vegetation. *Quarterly Journal of the Royal Meteorological Society*, *98*, 124–134.

Twine, T. E., Kustas, W., Norman, J., Cook, D. R., Houser, P. R., Meyers, T. P., ... Wesely, M. L. (2000). Correcting eddy-covariance flux underestimates over a grassland. *Agricultural and Forest Meteorology*, *103*, 279–300.

Urbanski, S., Barford, C., Wofsy, S., Kucharik, C., Pyle, E., Budney, J., ... Munger, J. W. (2007). Factors controlling CO_2 exchange on time-scales from hourly to decadal at Harvard Forest. *Journal of Geophysical Research: Biogeosciences*, *112*, G02020.

van Dijk, A. I., Gash, J. H., van Gorsel, E., Blanken, P. D., Cescatti, A., Emmel, C., ... Wohlfahrt, G. (2015). Rainfall interception and the coupled surface water and energy balance. *Agricultural and Forest Meteorology*, *214*, 402–415.

Verhoef, A., De Bruin, H., & Van Den Hurk, B. (1997). Some practical notes on the parameter kB^{-1} for sparse vegetation. *Journal of Applied Meteorology*, *36*, 560–572.

Verma, S. (1989). Aerodynamic resistances to transfers of heat, mass and momentum. In A. Black, D. Spittlehouse, M. Novak & D. Price (Eds.), *Estimation of areal evapotranspiration* (pp. 13–20). Wallingford, UK: International Association of Hydrological Sciences IAHS Publication No. 177.

Vesala, T., Suni, T., Rannik, U., Keronen, P., Markkanen, T., Sevanto, S., ... Hari, P. (2005). Effect of thinning on surface fluxes in a boreal forest. *Global Biogeochemical Cycles*, *19*, GB2001.

Wehr, R., Munger, J., McManus, J., Nelson, D. D., Zahniser, M. S., Davidson, E. A., ... Saleska, S. R. (2016). Seasonality of temperate forest photosynthesis and daytime respiration. *Nature*, *534*, 680–683.

Wilson, K., Goldstein, A., Falge, E., Aubinet, M., Baldocchi, D., Berbigier, P., ... Verma, S. (2002). Energy balance closure at FLUXNET sites. *Agricultural and Forest Meteorology*, *113*, 223–243.

Wohlfahrt, G., Bahn, M., Haslwanter, A., Newesely, C., & Cernusca, A. (2005). Estimation of daytime ecosystem respiration to determine gross primary production of a mountain meadow. *Agricultural and Forest Meteorology*, *130*, 13–25.

Wohlfahrt, G., & Gu, L. (2015). The many meanings of gross photosynthesis and their implication for photosynthesis research from leaf to globe. *Plant, Cell and Environment*, *38*, 2500–2507.

Wohlfahrt, G., Haslwanter, A., Hörtnagl, L., Jasoni, R. L., Fenstermaker, L. F., Arnone, J. A., & Hammerle, A. (2009). On the consequences of the energy imbalance for calculating surface conductance to water vapour. *Agricultural and Forest Meteorology*, *149*, 1556–1559.

Supporting Information for Knauer et al. – Global Change Biology

Authors: Jürgen Knauer*, Sönke Zaehle, Belinda E. Medlyn, Markus Reichstein, Christopher A. Williams, Mirco Migliavacca, Martin G. De Kauwe, Christiane Werner, Claudia Keitel, Pasi Kolari, Jean-Marc Limousin, Maj-Lena Linderson

*corresponding author (jknauer@bgc-jena.mpg.de)

A. Physically-based canopy boundary layer conductance model

The non-turbulent component of G_a is often expressed as the kB^{-1} parameter (Verhoef *et al.*, 1997; Massman, 1999), which is related to the boundary layer resistance (R_b) as follows (e.g. Verma, 1989):

$$R_b = \frac{kB^{-1}}{k\,u_*} \tag{S1}$$

where k is the von-Kármán constant (0.41), u_* is the friction velocity (m s^{-1}), and B^{-1} is the inverse Stanton number (Owen & Thomson, 1963). The kB^{-1} model used in this study (second term in Eq. (6)) was originally developed by Massman (1999), and simplified by Su *et al.* (2001):

$$kB^{-1} = \frac{k\,C_d}{4C_t \frac{u_*}{u(z_h)}} f_c^2 + kB_s^{-1}(1-f_c)^2 \tag{S2}$$

where C_d is a foliage drag coefficient, assumed constant with a value of 0.2 (Massman, 1999), C_t is the heat transfer coefficient of the leaf, $u(z_h)$ is the wind speed at canopy height (m s^{-1}), f_c is fractional canopy cover, and B_s^{-1} is the inverse Stanton number for bare soil surface (Su *et al.*, 2001). f_c was calculated from LAI for all sites:

$$f_c = \left(1 - \exp(-0.5\mathrm{LAI})\right) \tag{S3}$$

The kB^{-1} value for bare soil surface (kB_s^{-1}) is given by:

$$kB_s^{-1} = 2.46 * \text{Re}^{0.25} - \log(7.4) \tag{S4}$$

where Re is the Reynolds number for bare soil $\text{Re} = h_s u_* / v$ (Su *et al.*, 2001), where h_s is the roughness length of the soil, set to 0.01m, and v is the kinematic viscosity of air ($\text{m}^2 \text{ s}^{-1}$).Wind speed at canopy height $u(z_h)$ was calculated from the logarithmic wind profile equation:

$$u(z_h) = \frac{u_*}{k} \left(\ln \left[\frac{(z_h - d)}{z_{0m}} \right] - \psi_m \right) \tag{S5}$$

where z_r is measurement height (m) and ψ_m the integrated stability correction function for momentum (Paulson, 1970), which is a function of the stability parameter ζ ($\zeta = (z_r - d)/L$), where L is the Monin-Obukhov length. The zero-plane displacement height d (m) was fixed as a constant fraction of the canopy height ($d = 0.7z_h$), and the roughness length for momentum z_{0m} (m) was estimated from the following relation:

$$z_{0m} = (z_r - d) \exp(-ku/u_* - \psi_m) \tag{S6}$$

Note that z_{0m} as estimated from Eq. (S6) implicitly accounts for changes in z_r and/or d (along with e.g. an increase in canopy height), for which information was not available on an annual basis. As a consequence, z_{0m} in this study has to be interpreted as an effective parameter, integrating any changes in the aerodynamic properties of the ecosystem.

The heat transfer coefficient C_t is given by:

$$C_t = \text{Pr}^{-2/3} \text{Re}_h^{-1/2} N \tag{S7}$$

where N is the number of leaf sides participating in heat transfer (Massman, 1999), Pr is the Prandtl number (0.71), and Re_h is the Reynolds number, defined as:

$$\text{Re}_h = D_l u/v \tag{S8}$$

where D_l is the characteristic leaf dimension (m), which was approximated by the geometric mean of the average leaf width and leaf length of the dominant species at the site (Table S1). N in Eq. S7 was set to 2 for both water vapor and heat, thus assuming that both kB^{-1} and R_b are equal for the two scalars. This is one assumption made in the PM equation (Eq. (2)), which was supported experimentally (Verma, 1989).

B. Random forest model

The random forest algorithm is implemented in R using the *randomForest* package (Liaw & Wiener, 2002). The following regression model was constructed:

$$G_1 \sim \text{EBR}_{\text{halfhourly}} + \lambda E + \text{PPFD} + T_0 + G_{\text{a,empGb}} + \text{DOY} + \text{hour} + G_{\text{c,layer}}/G_{\text{c,tot}}$$

where DOY is day of year. The focus was on the relationship between G_1 and the fraction of G_c coming from a certain layer (i.e. $G_{\text{c,layer}}/G_{\text{c,tot}}$ as a proxy for the contribution of $G_{1,\text{layer}}$ to total G_1). The marginal effect of $G_{\text{c,layer}}/G_{\text{c,tot}}$ on G_1 was calculated with the function *partialPlot()*.

Tables

Table S1: Basic observed and calculated aerodynamic properties of the sites investigated in this study. (z_h = mean canopy height; ζ = stability parameter; D_l = characteristic leaf dimension; R_{aM} = aerodynamic resistance for momentum; $R_{b,empGb}$ = canopy boundary layer resistance for heat, calculated according to Thom (1972); $R_{b,physGb}$ = canopy boundary layer resistance for heat, calculated according to Su *et al.* (2001); $kB^{-1}_{,physGb}$ = kB^{-1} parameter, calculated according to Su *et al.* (2001); $R_{a,empGb}$ = total aerodynamic resistance for heat, calculated according to Eq. 5 in the main manuscript; $R_{a,physGb}$ = total aerodynamic resistance for heat, calculated according to Eq. 6 in the main manuscript). Shown are median values over all site years. Data were filtered as described in the Materials and methods section.

Site	z_h (m)	ζ	D_l (m)	R_{aM} (s m^{-1})	$R_{b,empGb}$ (s m^{-1})	$R_{b,physGb}$ (s m^{-1})	$kB^{-1}_{,physGb}$	$R_{a,empGb}$ (s m^{-1})	$R_{a,physGb}$ (s m^{-1})
AU-Tum	40	-0.20	0.06	5.95	7.63	5.02	1.64	13.70	11.11
DK-Sor	25	-0.08	0.06	9.43	8.06	10.64	3.13	17.54	20.41
FI-Hyy	14	-0.08	0.01	10.10	8.55	4.74	1.26	18.52	14.92
FR-Pue	5.5	-0.07	0.03	10.53	9.17	5.31	1.34	20.00	16.13
GF-Guy	35	-0.17	0.06	9.43	8.47	11.24	3.09	17.86	20.83
US-Ha1	23	-0.07	0.10	6.80	9.01	7.35	1.95	15.87	13.89

**Table S2:** Standard error of the regression (SER) for all sites and multiple model versions.

G_1 version[a]	AU-Tum	DK-Sor	FI-Hyy	FR-Pue	GF-Guy	US-Ha1
fcoupled, air, nt	0.160	0.156	0.065	0.052	0.185	0.159
empGb, air, nt	0.171	0.228	0.070	0.046	0.255	0.166
physGb, air, nt	0.169	0.238	0.067	0.045	0.268	0.169
empGb, surface, nt	0.167	0.211	0.065	0.044	0.248	0.161
physGb, surface, nt	0.166	0.226	0.064	0.044	0.263	0.164
empGb, surface, dt	0.175	0.231	0.076	0.049	0.255	0.169
physGb, surface, dt	0.173	0.245	0.076	0.050	0.272	0.173

[a] denoted as: G_a formulation, air or surface conditions, nighttime (nt) or daytime (dt) NEE-partitioning.

Figures
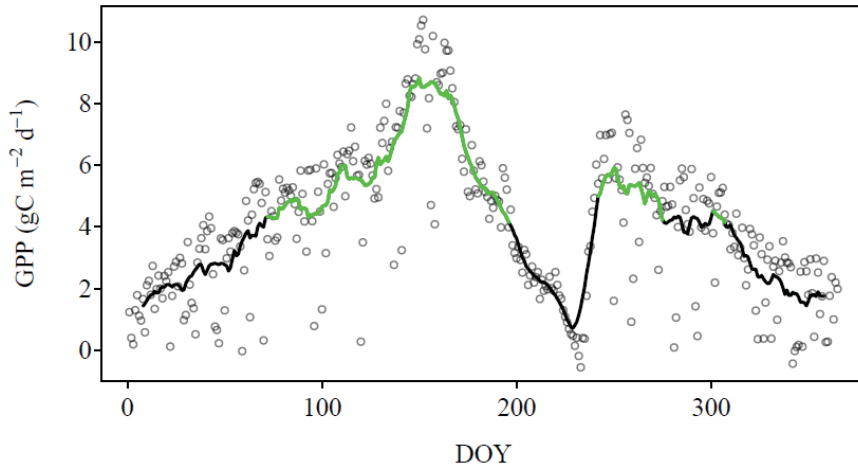
Figure S1 GPP-based growing season filter used in this study shown for the site FR-Pue for the year 2002. Grey dots are daily GPP sums, the black line is the smoothed GPP time series (window width = 15 days), and the green line is the time period that was considered to be in the growing season.
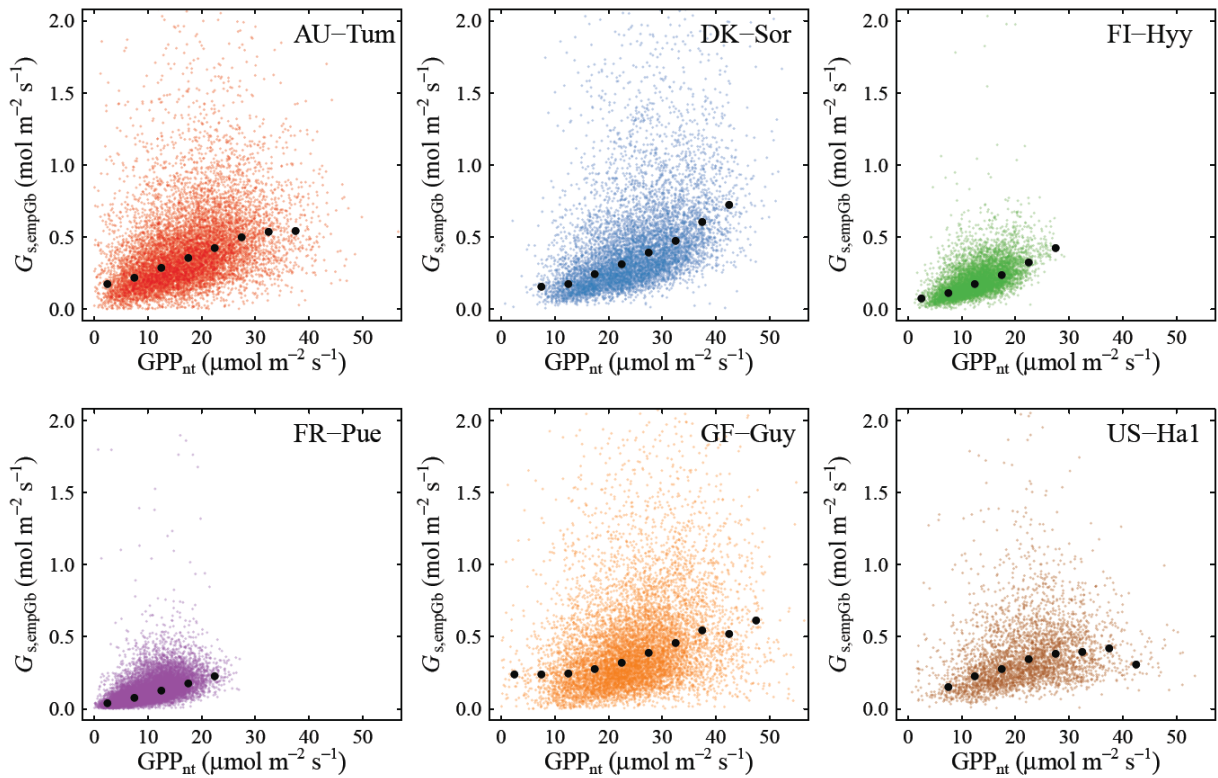

Figure S2 Surface conductance (G_s, calculated using the G_a version $G_{a,empGb}$ (Eq. (5)) plotted against GPP (derived from NEE using the nighttime approach according to Reichstein *et al.* (2005)). Black dots indicate the median of the respective bins.
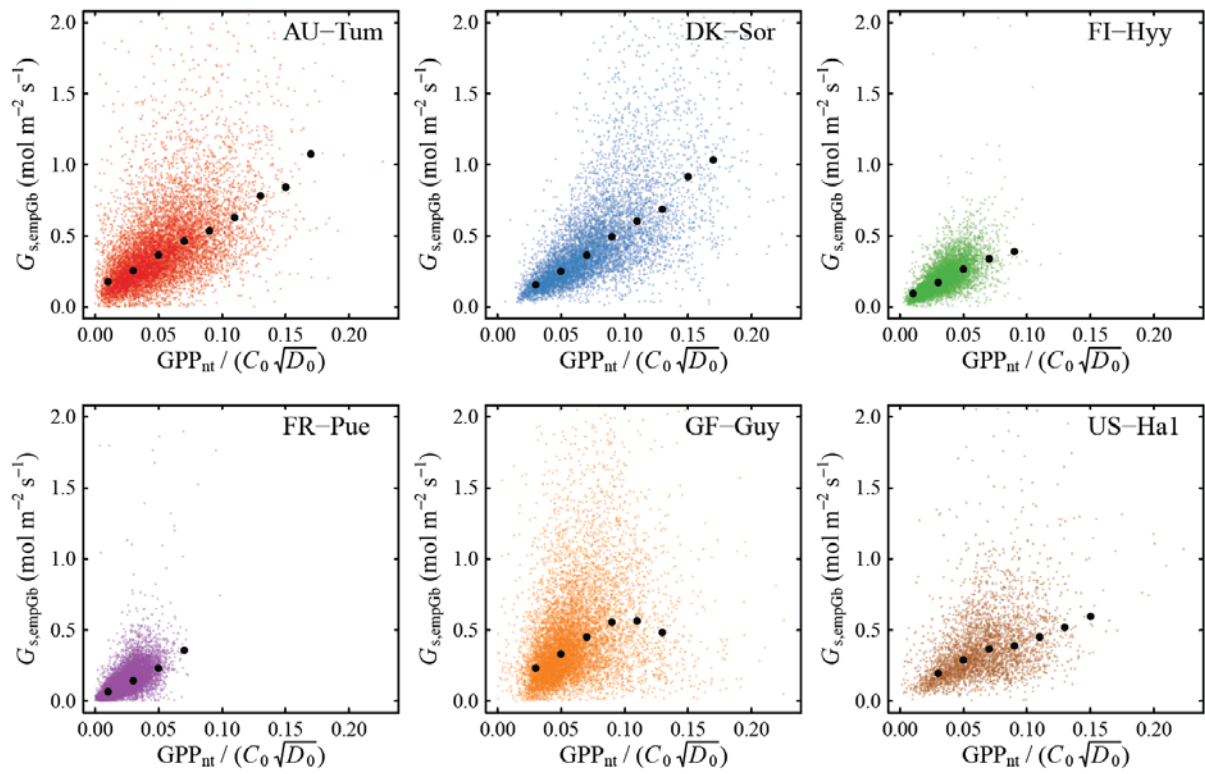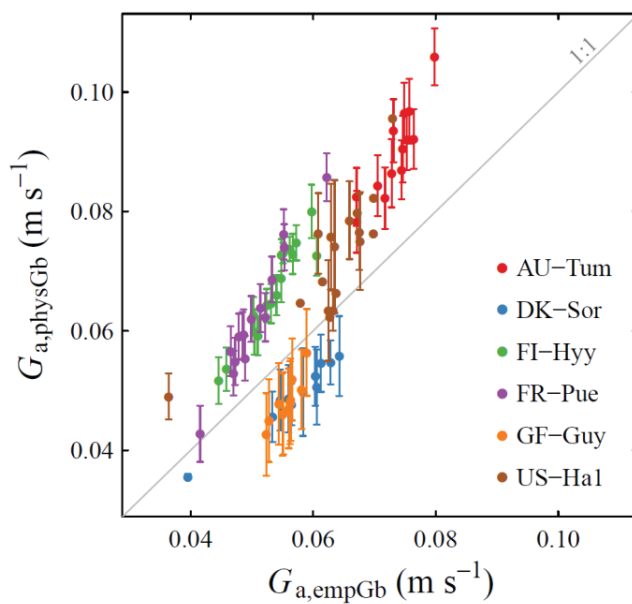
Figure S3 Surface conductance (G_s, calculated using the G_a version $G_{a,empGb}$ (Eq. (5)) plotted against GPP / ($C_0 \sqrt{D_0}$) (with GPP derived from NEE using the nighttime approach according to Reichstein *et al.* (2005)). Black dots indicate the median of the respective bins.
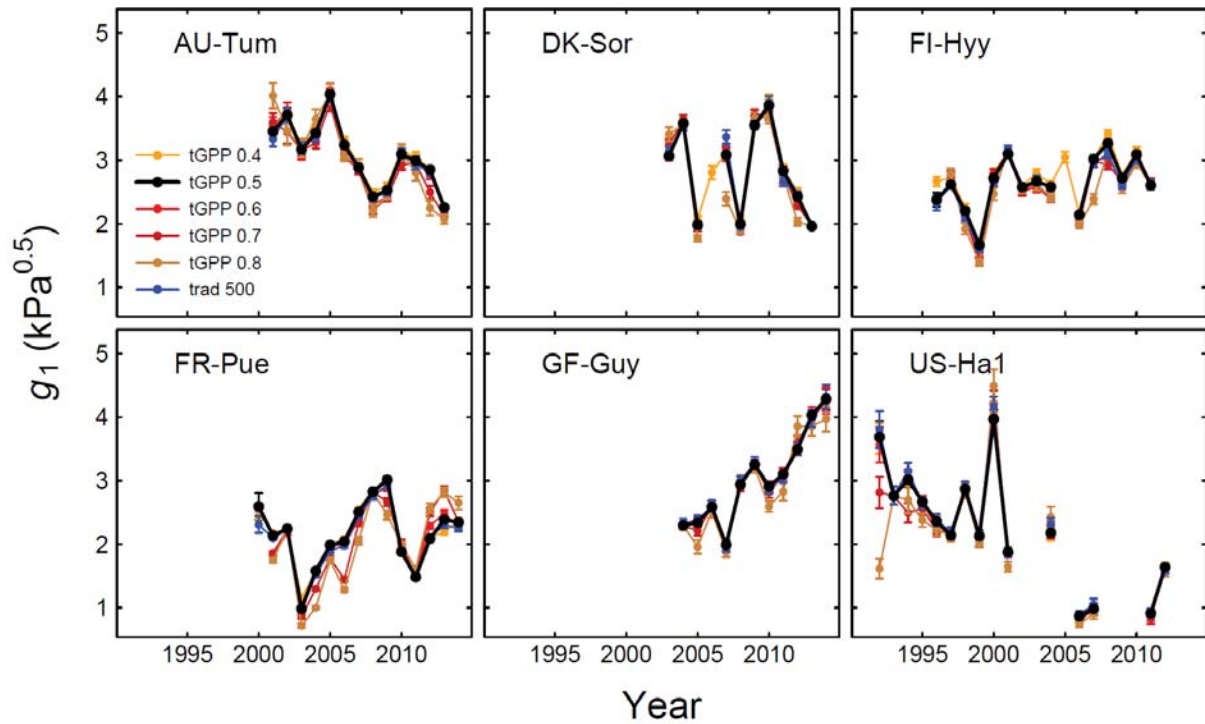
Figure S4 Sensitivity of annual G_1 estimates to alternative data filters with respect to growing season and radiation thresholds. *tGPP 0.4*, *tGPP 0.5*, *tGPP 0.6*, *tGPP 0.7*, and *tGPP 0.8* denote GPP thresholds corresponding to 40, 50, 60, 70, and 80%, respectively, of the 95th percentile of smoothed daily GPP time series, above which the data were considered to be in the growing season (see Fig. S1). *trad 500* denotes an increased radiation threshold of 500 μmol m^{-2} s^{-1}. The thick black line denotes the filter as applied in this study (GPP threshold of 0.5 (50%) and radiation threshold of 200 μmol m^{-2} s^{-1}). Error bars indicate standard errors.
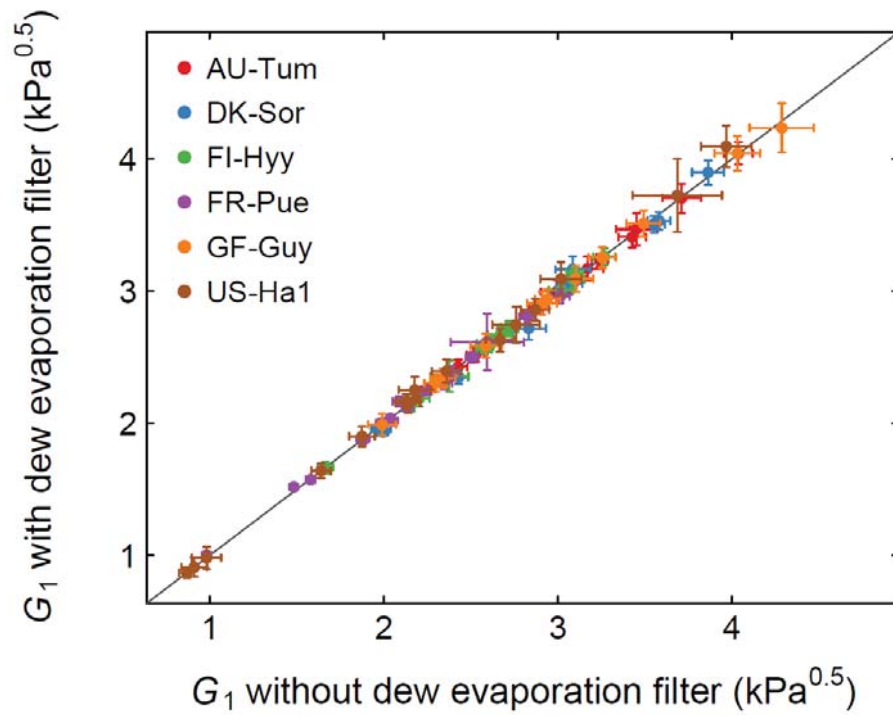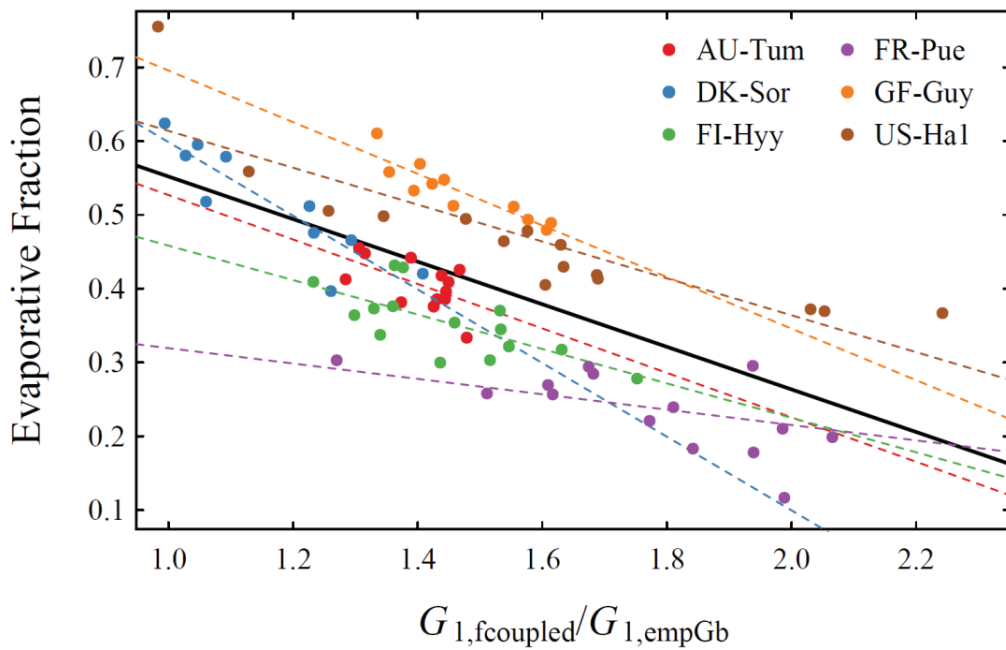
Figure S5 Effect of the implemented dew evaporation filter on the estimated G_1. The filter excludes time periods that have a high probability of being affected by dew evaporation.


Figure S6 Comparison of median annual values of aerodynamic conductance (G_a) calculated from different formulations (Eqs. (5,6)).
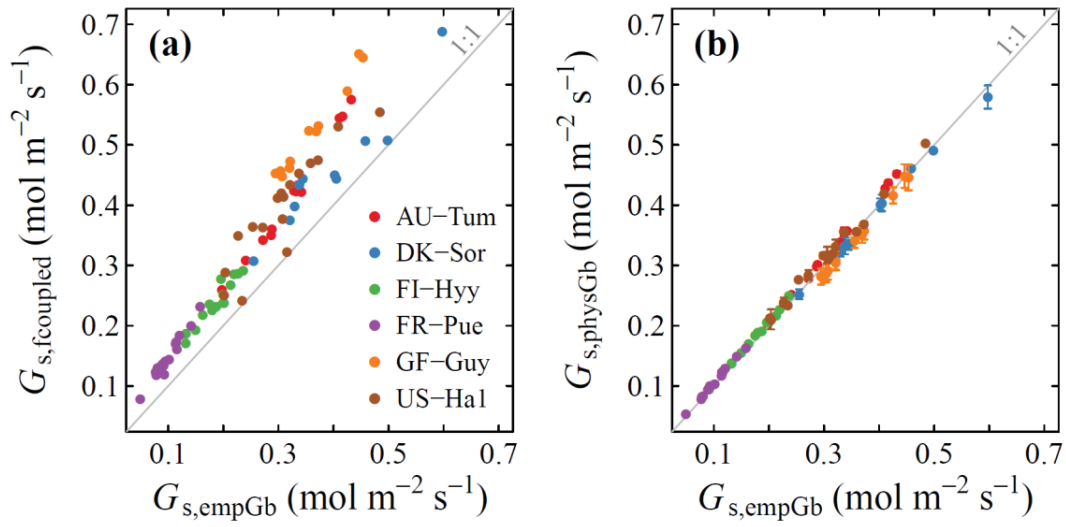
Figure S7 Same as Figure S for surface conductance (G_s).

Figure S8 The relation between evaporative fraction ($\lambda E/R_n$) and the effects of G_a on the estimated G_1. Dashed colored lines and the bold black line are ordinary least squares fits for individual sites and all sites, respectively.
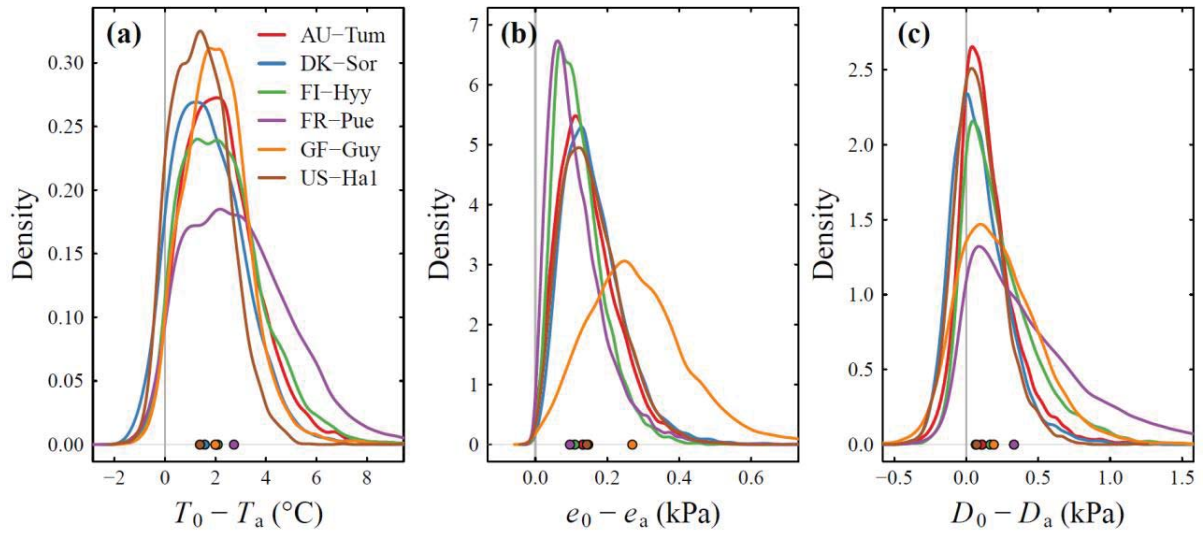
Figure S9 Deviations of **(a)** Canopy surface temperature, **(b)** vapor pressure, and **(c)** the resulting vapor pressure deficit (as in Fig. 4) from those measured in the air. Surface conditions are derived from inverted bulk transfer equations (Eqs. (7) - (9)) with G_a estimated from Eq. (5).
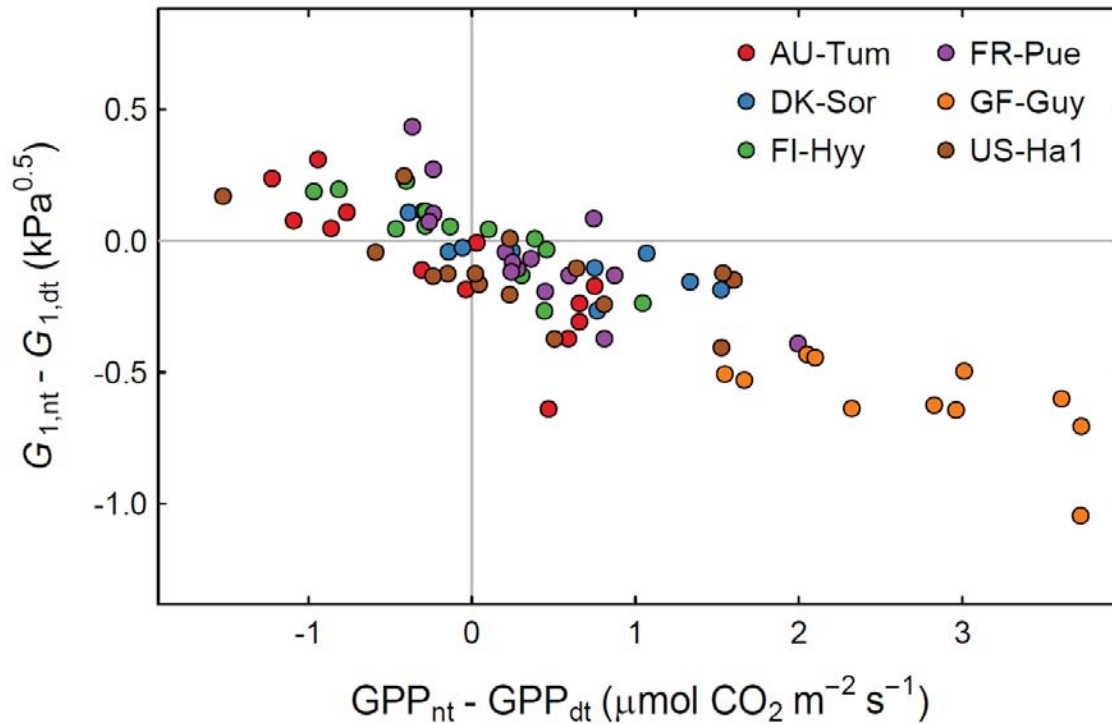
Figure S10 Differences in GPP as a result of the two different NEE partitioning algorithms (nighttime approach (Reichstein *et al.*, 2005) and daytime approach (Lasslop *et al.*, 2010)) and their effects on G_1.

References

Lasslop G, Reichstein M, Papale D *et al.* (2010) Separation of net ecosystem exchange into assimilation and respiration using a light response curve approach: critical issues and global evaluation. *Global Change Biology,* **16**, 187-208.

Liaw A, Wiener M (2002) Classification and Regression by randomForest. *R News,* **2**, 18-22.

Massman W (1999) A model study of kB_H^{-1} for vegetated surfaces using 'localized near-field' Lagrangian theory. *Journal of Hydrology,* **223**, 27-43.

Owen P, Thomson W (1963) Heat transfer across rough surfaces. *Journal of Fluid Mechanics,* **15**, 321-334.

Paulson CA (1970) The mathematical representation of wind speed and temperature profiles in the unstable atmospheric surface layer. *Journal of Applied Meteorology,* **9**, 857-861.

Reichstein M, Falge E, Baldocchi D *et al.* (2005) On the separation of net ecosystem exchange into assimilation and ecosystem respiration: review and improved algorithm. *Global Change Biology,* **11**, 1424-1439.

Su Z, Schmugge T, Kustas W, Massman W (2001) An evaluation of two models for estimation of the roughness height for heat transfer between the land surface and the atmosphere. *Journal of Applied Meteorology,* **40**, 1933-1951.

Thom A (1972) Momentum, mass and heat exchange of vegetation. *Quarterly Journal of the Royal Meteorological Society,* **98**, 124-134.

Verhoef A, De Bruin H, Van Den Hurk B (1997) Some practical notes on the parameter kB^{-1} for sparse vegetation. *Journal of Applied Meteorology,* **36**, 560-572.

Verma S (1989) Aerodynamic resistances to transfers of heat, mass and momentum. In: *Estimation of areal evapotranspiration.* (eds Black A, Spittlehouse D, Novak M, Price D), pp 13-20, IAHS Publication No. 177.